[2] Tissenbaum, H.A. and Guarente, L. (2001) Increased dosage of a sir-2 gene extends lifespan in *Caenorhabditis elegans*. Nature 410, 227–230.
[3] Rogina, B. and Helfand, S.L. (2004) Sir2 mediates longevity in the fly through a pathway related to calorie restriction. Proc. Natl. Acad. Sci. USA 101, 15998–16003.
[4] Colman, R.J., Anderson, R.M., Johnson, S.C., Kastman, E.K., Kosmatka, J.K., Beasley, T.M., Allison, D.B., Cruzen, C., Simmons, H.A., Kemnitz, J.W. and Weindruch, R. (2009) Caloric restriction delays disease onset and mortality in rhesus monkeys. Science 325 (5937), 201–204.
[5] Kaeberlein, M., McVey, M. and Guarente, L. (1999) The SIR2/3/4 complex and SIR2 alone promote longevity in *Saccharomyces cerevisiae* by two different mechanisms. Genes Dev. 13, 2570–2580.
[6] Du, J., Zhou, Y., Su, X., Yu, J.J., Khan, S., Jiang, H., Kim, J., Woo, J., Kim, J.H., Choi, B.H., He, B., Chen, W., Zhang, S., Cerione, R.A., Auwerx, J., Hao, Q. and Lin, H. (2011) Sirt5 is a NAD-dependent protein lysine demalonylase and desuccinylase. Science 334 (6057), 806–809.
[7] Satoh, A., Stein, L. and Imai, S. (2011) The role of mammalian sirtuins in the regulation of metabolism, aging, and longevity. Handb. Exp. Pharmacol. 206, 125–162.
[8] Nakamura, Y., Ogura, M., Tanaka, D. and Inagaki, N. (2008) Localization of mouse mitochondrial SIRT proteins: shift of SIRT3 to nucleus by co-expression with SIRT5. Biochem. Biophys. Res. Commun. 366 (1), 174–179.
[9] Michishita, E., Park, J.Y., Burneskis, J.M., Barrette, J.C. and Horikawa, I. (2005) Evolutionarily conserved and nonconserved cellular localizations and functions of human SIRT proteins. Mol. Biol. Cell 16 (10), 4623–4635.
[10] Schlicker, C., Gertz, M., Papatheodorou, P., Kachholz, B., Becker, C.F. and Steegborn, C. (2008) Substrates and regulation mechanisms for the human mitochondrial sirtuins Sirt3 and Sirt5. J. Mol. Biol. 382 (3), 790–801.
[11] Peng, C., Lu, Z., Xie, Z., Cheng, Z., Chen, Y., Tan, M., Luo, H., Zhang, Y., He, W., Yang, K., Zwaans, B.M., Tishkoff, D., Ho, L., Lombard, D., He, T.C., Dai, J., Verdin, E., Ye, Y. and Zhao, Y. (2011) The first identification of lysine malonylation substrates and its regulatory enzyme. Mol. Cell. Proteomics 10 (12). M111.012658.
[12] Ogura, M., Nakamura, Y., Tanaka, D., Zhuang, X., Fujita, Y., Obara, A., Hamasaki, A., Hosokawa, M. and Inagaki, N. (2010) Overexpression of SIRT5 confirms its involvement in deacetylation and activation of carbamoyl phosphate synthetase 1. Biochem. Biophys. Res. Commun. 393 (1), 73–78.
[13] Nakagawa, T., Lomb, D.J., Haigis, M.C. and Guarente, L. (2009) SIRT5 deacetylates carbamoyl phosphate synthetase 1 and regulates the urea cycle. Cell 137 (3), 560–570.
[14] Álvarez-Lario, B. and Macarrón-Vicente, J. (2010) Uric acid and evolution. Rheumatology 49 (11), 2010–2015.
[15] Wu, X.W., Muzny, D.M., Lee, C.C. and Caskey, C.T. (1992) Two independent mutational events in the loss of urate oxidase during hominoid evolution. J. Mol. Evol. 34 (1), 78–84.
[16] Nakamura, Y., Suzuki, H., Sakaguchi, M. and Mihara, K. (2004) Targeting and assembly of rat mitochondrial translocase of outer membrane 22 (TOM22) into the TOM complex. J. Biol. Chem. 279 (20), 21223–21232.
[17] Priest, D.G. and Pitts, O.M. (1972) Reaction intermediate effects on the spectrophotometric uricase assay. Anal. Biochem. 50 (1), 195–205.
[18] Yokota, S. (1973) Studies on mouse liver urate oxidase II. Immunochemical and enzymatic distribution of urate oxidase in mouse liver cell fractions. Histochemie 37, 149–159.
[19] Kim, S.C., Sprung, R., Chen, Y., Xu, Y., Ball, H., Pei, J., Cheng, T., Kho, Y., Xiao, H., Xiao, L., Grishin, N.V., White, M., Yang, X.J. and Zhao, Y. (2006) Substrate and functional diversity of lysine acetylation revealed by a proteomics survey. Mol. Cell 23 (4), 607–618.
[20] Yeldandi, A.V., Chu, R., Pan, J., Zhu, Y. and Usuda, Y. (1996) Peroxisomal purine metabolism. Ann. N. Y. Acad. Sci. 804, 165–175.
[21] Wu, X., Wakamiya, M., Vaishnav, S., Geske, R., Montgomery, C., Jones, P., Bradley, A. and Caskey, C.T. (1994) Hyperuricemia and urate nephropathy in urate oxidase-deficient mice. Proc. Natl. Acad. Sci. USA 91 (2), 742–746.
[22] Freitas, S., Spencer, P.J., Vassão, R.C. and Abrahão-Neto, J. (2010) Biochemical and biopharmaceutical properties of PEGylated uricase. Int. J. Pharm. 387 (1–2), 215–222.
[23] Malaguarnera, G., Giordano, M. and Malaguarnera, M. (2012) Rasburicase for the treatment of tumor lysis in hematological malignancies. Expert Rev. Hematol. 5 (1), 27–38.
[24] Pession, A., Melchionda, F. and Castellini, C. (2008) Pitfalls, prevention, and treatment of hyperuricemia during tumor lysis syndrome in the era of rasburicase (recombinant urate oxidase). Biologics 2 (1), 129–141.

Human Molecular Genetics, 2012, Vol. 21, No. 4 **765–775**
doi:10.1093/hmg/ddr508
Advance Access published on November 7, 2011

Molecular and cellular characteristics of *ABCA3* mutations associated with diffuse parenchymal lung diseases in children

Florence Flamein[1], Laure Riffault[1], Céline Muselet-Charlier[1], Julie Pernelle[1], Delphine Feldmann[3], Laurence Jonard[3], Anne-Marie Durand-Schneider[1], Aurore Coulomb[4], Michèle Maurice[1], Lawrence M. Nogee[6], Nobuya Inagaki[7], Serge Amselem[2], Jean Christophe Dubus[8], Virginie Rigourd[9], François Brémont[10], Christophe Marguet[11], Jacques Brouard[12], Jacques de Blic[13], Annick Clement[1,5], Ralph Epaud[14,15] and Loïc Guillot[1,*]

[1]Inserm U938 and [2]Inserm U933, UPMC, Univ Paris 6, France, [3]Department of Biochemistry, [4]Department of Pathology and [5]Department of Pediatric Pulmonology, Reference Center for Rare Respiratory Diseases in Children, Armand Trousseau Hospital, AP-HP, Paris, France, [6]Division of Neonatology, Department of Pediatrics, Johns Hopkins University School of Medicine, Baltimore, MD, USA, [7]Department of Diabetes and Clinical Nutrition, Graduate School of Medicine, Kyoto University, Kyoto, Japan, [8]Department of Pediatrics, Timone University Hospital, Marseille, France, [9]Institut de Puériculture de Paris, Paris, France, [10]Department of Pediatric Pulmonology and Allergology, Centre Hospitalo-Universitaire (CHU), Toulouse, France, [11]Department of Pediatric Pulmonology and Allergology, CHU, Charles Nicolle, Rouen, France, [12]Department of Pediatrics, CHU de Caen, Caen, France, [13]Department of Pediatric Pulmonology-Allergology, Université Paris Descartes, Hôpital Necker Enfants Malades, AP-HP, Paris, France, [14]Inserm U955, Créteil, France and [15]Université Paris Est, Créteil, France

Received August 29, 2011; Revised and Accepted October 29, 2011

ABCA3 (ATP-binding cassette subfamily A, member 3) is expressed in the lamellar bodies of alveolar type II cells and is crucial to pulmonary surfactant storage and homeostasis. *ABCA3* gene mutations have been associated with neonatal respiratory distress (NRD) and pediatric interstitial lung disease (ILD). The objective of this study was to look for *ABCA3* gene mutations in patients with severe NRD and/or ILD. The 30 *ABCA3* coding exons were screened in 47 patients with severe NRD and/or ILD. *ABCA3* mutations were identified in 10 out of 47 patients, including 2 homozygous, 5 compound heterozygous and 3 heterozygous patients. SP-B and SP-C expression patterns varied across patients. Among patients with *ABCA3* mutations, five died shortly after birth and five developed ILD (including one without NRD). Functional studies of p.D253H and p.T1173R mutations revealed that p.D253H and p.T1173R induced abnormal lamellar bodies. Additionally, p.T1173R increased IL-8 secretion *in vitro*. In conclusion, we identified new *ABCA3* mutations in patients with life-threatening NRD and/or ILD. Two mutations associated with ILD acted via different pathophysiological mechanisms despite similar clinical phenotypes.

INTRODUCTION

Pulmonary surfactant, a complex mixture of lipids and specific proteins located at the air–liquid interface, lowers alveolar surface tension, thereby preventing alveolar collapse at the end of expiration. It is synthesized by alveolar type-II cells, stored in lamellar bodies and secreted by exocytosis. Phospholipids make up ~90% of pulmonary surfactant.

Recent studies indicate a role for several genes in diffuse lung diseases (1–3). Genes implicated to date include the

*To whom correspondence should be addressed at: INSERM U938, Bâtiment Kourilsky, 184 rue du Faubourg Saint Antoine, 75012 Paris, France. Tel: +33 149284682; Fax: +33 143401748; Email: loic.guillot@inserm.fr

Table 1. Genetic analysis results in the 10 children harboring homozygous and compound heterozygous (shaded) or heterozygous *ABCA3* mutations

Patient	NRD	Clinical outcome	*ABCA3* mutation cDNA level	Protein level	*ABCA3* SNPs dbSNPs rs# cluster id	*ABCA3* variants Missense variants in conserved amino acid
1	Yes	ILD	c.[3518C>G] + [3518C>G]	p.[T1173R] + [T1173R]	rs149532, rs13332514	
2	Yes	ILD	c.[757G>C] + [757G>C]	p.[D253H] + [D253H]		
3	Yes	Death	c.[1385T>G] + [2890G>A]	p.[L462R] + [G964S]	rs149532	
4	Yes	Death	c.[4747C>T] + c.[384delC]	p.[R1583W] + p.[S128Rfs]	rs149532	c.[450G>A] (het)
5	No	Death	c.[629G>T] + [3079G>C]	p.[G210V] + [A1027P]	rs149532	
6	Yes	ILD	c.[622C>T] + [4561C>T]	p.[R208W] + [R1521W]	rs149532, rs323043	
7	Yes	Death	c.[604G>C] + [907C>G]	p.[G202R] + [L303V]	rs149532, rs323043 (het), rs13332514	
8	Yes	Death	c.[2888A>G] + [?]	p.[Y963C] + [?]	rs149532 (het), rs323043 (het)	
9	Yes	ILD	c.[2125C>T] + [?]	p.[R709W] + [?]	rs149532	
10	Yes	ILD	c.[2614A>G] + [?]	p.[S872G] + [?]	rs149532 (het), rs323043, rs13332514 (het)	

het, heterozygous; NRD, neonatal respiratory distress; ILD, interstitial lung disease.

surfactant protein (SP)-B and SP-C genes (*SFTPB*, MIM 178640; and *SFTPC*, MIM 178620) and the ATP-binding cassette subfamily A member 3 gene (*ABCA3*, MIM 601615). SP-B deficiency has long been known to cause lethal neonatal respiratory distress (NRD) (4). More recently, *SFTPC* mutations were reported in newborns and infants with severe alveolar-interstitial syndrome (3,5). ABCA3 is a 1704-amino acid protein expressed selectively—but not specifically—in the lung, where it is found in the limiting membrane of lamellar bodies (1,6,7). ABCA3 is encoded by an 80 kb gene mapped to 16p13.3 in humans and is thought to regulate lipid transport and organization during lamellar body formation (8,9).

ABCA3 gene mutations are transmitted by autosomal recessive inheritance. As with SP-B deficiency, ABCA3 deficiency should be suspected in full-term infants with severe NRD refractory to maximal conventional treatment (10,11). In addition, *ABCA3* gene mutations have been found in children and young adults with interstitial lung disease (ILD) (1,3,12). For instance, the heterozygous c.875A>T (p.Glu292Val, p.E292V) *ABCA3* mutation was identified in several older children and young adults with desquamative interstitial pneumonitis (1). The large size and marked allelic heterogeneity of the *ABCA3* gene create challenges in mutation identification.

The objectives of this study were to identify and characterize *ABCA3* variations in a large population of pediatric patients with NRD and/or ILD. We identified new *ABCA3* gene mutations and found that these mutations were not associated with a specific expression profile of SP-B and SP-C in bronchoalveolar lavage fluid (BALF). Functional analysis of two mutations associated with ILD showed different pathophysiological mechanisms, despite the similar clinical phenotype.

RESULTS

Study patients

Of the 47 children enrolled in the study (Supplementary Material, Supporting Information 1), 23 (49%) were male and 24 (51%) female. The patients were from Europe ($n = 27$), North Africa ($n = 12$), Reunion Island ($n = 6$), West Africa ($n = 1$) and Haiti ($n = 1$). Among them, 6 (13%) were born prematurely (<36 weeks) and 31 (66%) had NRD. ILD developed in 31 (66%) patients, and 21 (36%) patients had both NRD and ILD. Nine (19%) patients died of respiratory failure.

Genetic analysis

Of the 47 patients, 10 had *ABCA3* mutations. We identified 15 mutations, including 13 that had not been described previously. The two mutations p.G210V and p.R208W have been already identified (13,14). There were 14 missense mutations and 1 heterozygous nonsense mutation (p.Ser128ArgfsX23, designated hereafter as p.S128Rfs) (Table 1).

Analysis of genomic DNA from the parents and kindred showed that the compound heterozygous p.R1583W/p.S128Rfs (Fig. 1A) and p.R208W/p.R1521W (Fig. 1B) mutations were inherited, as well as the homozygous mutations p.T1173R (Fig. 1C) and p.D253H (Fig. 1D). For the other mutations, genomic DNA samples from family members were not available.

None of these newly identified *ABCA3* mutations has been previously described as polymorphisms (http://ncbi.nih.gov/SNP). In addition, none of the new variants was detected in the 46 alleles from our 23 controls. Alignment of the human and other mammalian amino acid sequences (by Multiple Sequence Comparison using Log-Expectation, MUSCLE analysis) indicated that almost all the *ABCA3* mutations occurred in highly conserved residues (not illustrated). They were located across the protein in the extracellular domains (ECD1 and ECD2), as well as in internal domains (NBD1 and NBD2) (Fig. 2). Finally, complete *ABCA3* sequencing disclosed previously described single-nucleotide polymorphisms (SNPs) (Table 1), as well as a missense variant affecting a conserved amino acid in the patient harboring the c.[4747C>T]+[384delC] mutation.

In the 37 patients without *ABCA3* mutations, four SNPs were identified in the coding region of *ABCA3*. These SNPs were in exons 7, 9, 14 and 26, respectively, and did not induce amino acid variations. A missense variant in the conserved amino acid c.1059C>T was identified in nine children. We found these variants neither in the public polymorphism database nor in our controls.

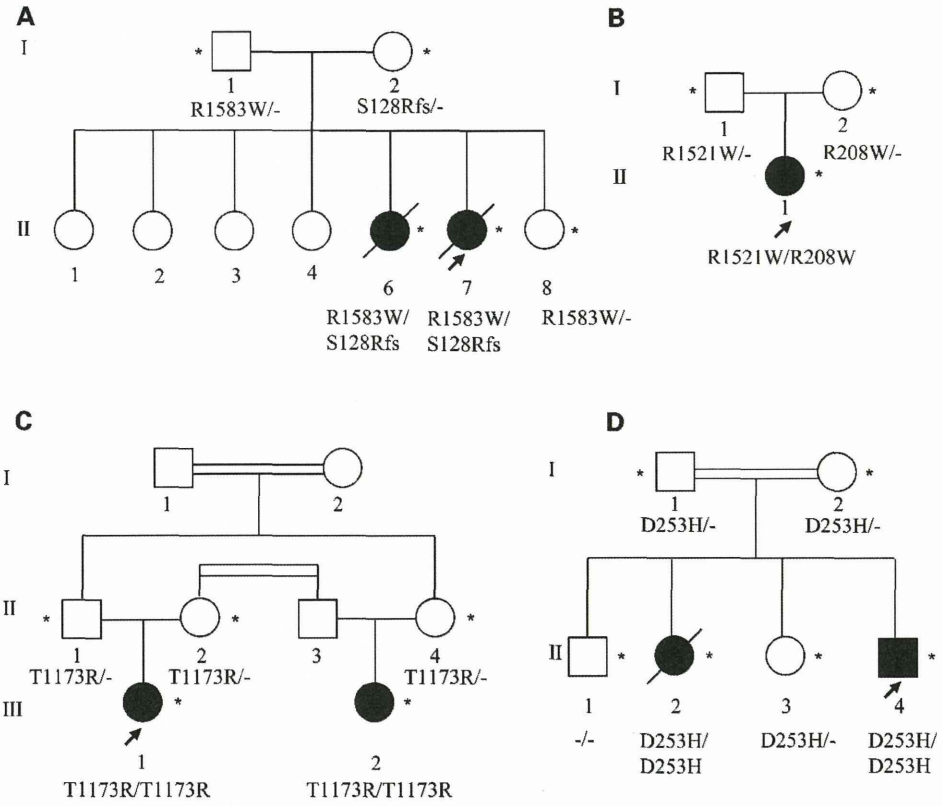

Figure 1. Pedigree of the families with the *ABCA3* mutations p.R1583W/p.S128Rfs (**A**), p.R1521W/R208W (**B**), p.T1173R/p.T1173R (**C**) and p.D253H/p.T1173R (**D**). Asterisks indicate family members with ABCA3 mutation analysis, and arrows indicate index patients.

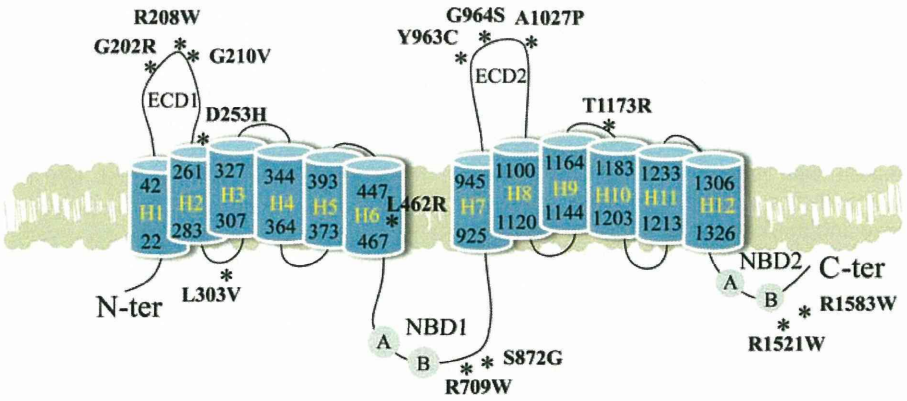

Figure 2. Schematic representation of the ABCA3 protein [N-terminal (N-ter) to C-terminal (C-ter) domains] and the location of the novel mutations (indicated by an asterisk). The 12 putative transmembrane helix (H1–H12) domains, two extracellular domains (ECD1 and ECD2) and two nucleotide-binding domains (NBD) (including the conserved motifs Walker A and B) are represented.

Characteristics of patients with *ABCA3* mutations

The characteristics of the 10 children with ABCA3 mutations are reported in Table 2. Among them, nine (90%) had NRD, five progressed to ILD and five died of respiratory failure (all during the first year of life).

Three children harboring homozygous and compound heterozygous mutations who developed ILD (patients 1, 2 and 6) were treated with methylprednisolone pulse for, respectively, 14 months (patient 1), 6 years (patient 2) and 11 years (patient 6, who is still on methylprednisolone pulse). They also received azithromycin for, respectively, 2 years (patient 1), 12 years (patient 2) and 2 years (patient 6), patients 2 and 6 still being treated. Two patients (patients 2 and 6) required prolonged oxygen supplementation for, respectively, 10 years (patient 2) and 11 years (patient 6, who is still on oxygen).

Two children harboring heterozygous mutations developed ILD (patients 10 and 9). The first child (patient 10) was

Table 2. Clinical characteristics of the 10 patients with *ABCA3* mutations

	ABCA3-mutated patients ($n = 10$)
Sex: male/female, *n* (%)	4 (40)/6 (60)
Median age at onset in months (range)	0 (0–6)
Neonatal respiratory distress, *n* (%)	9 (90)
Hypoxemia, *n* (%)	10 (100)
Physical findings, *n* (%)	
Tachypnea	10 (100)
Retractions	10 (100)
HRCT findings, *n* (%)	
Ground-glass opacities	8 (100)
Lung cysts	3 (38)
Interlobular septal thickening	2 (25)
Consolidation	4 (50)
Lung biopsy, *n* (%)	
Type-II cell hyperplasia	6 (100)
Septal thickening	6 (100)
Mild fibrosis	5 (83)
Intra-alveolar macrophages	6 (100)
Outcome *n* (%)	
ILD/death	5 (50)/5 (50)

ILD, interstitial lung disease; *n* corresponds to the number of available patients' clinical data.

treated by monthly methylprednisolone pulse for 3 years and required oxygen supplementation for 8 months. The second one (patient 9) did not receive any treatment during the study period.

All 10 patients had clinical symptoms of respiratory failure. High-resolution computed tomography (HRCT) scans were available for eight patients and predominantly showed ground-glass opacities (Fig. 3A and Supplementary Material, Supporting Information 2). Lung biopsy was performed in six patients, all of whom had alveolar septal thickening, a few interstitial inflammatory cells (polymorphonuclear neutrophils and lymphocytes), uniform prominent type-II cell hyperplasia and accumulation of intra-alveolar macrophages (Fig. 3B). Electron microscopy was performed on a lung biopsy from the patient harboring the p.D253H mutation and showed abnormal lamellar bodies with dense inclusions (Fig. 3C).

BALF analysis

Western blot analysis of surfactant proteins (Fig. 4) was performed in seven patients, who had the following *ABCA3* mutations: p.D253H (patient 2), p.T1173R (patient 1), p.L462R/p.G964S (patient 3), p.G202R/p.L303V (patient 7), p.Y963C (patient 8), p.R1583W/p.S128Rfs (patient 4) and p.S872G (patient 10), respectively. SP-C (Fig. 4A) and SP-B (Fig. 4B) were detected at a size of 3.7 and 8 kDa in variable amounts, the smallest amount being found in the patient with the p.G202R/p.L303V *ABCA3* mutation (patient 7) in whom SP-C and SP-B are only faintly visible. This patient was the only one who cannot be weaned off mechanical ventilation before he died of respiratory failure. Interestingly, the two children harboring homozygous mutations (patients 1 and 2) have small but detectable amounts, which were nonetheless compatible with life. In contrast, patient 4, who died within the first month of life, had amount of SP-B and SP-C similar to control.

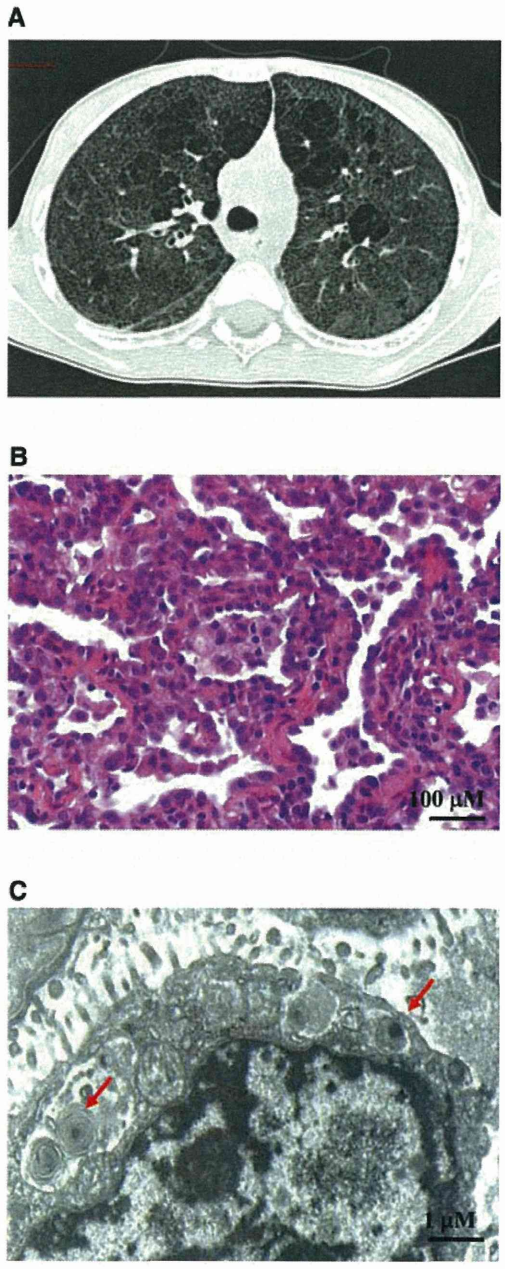

Figure 3. (**A**) HRCT scan, (**B**) hematoxylin and eosin (HE) staining of lung tissue and (**C**) electron microscopy of type-II cells from the patient (patient 2) harboring the *ABCA3* homozygous mutation p.D253H. Red arrows indicate lamellar bodies.

Characterization of ABCA3 mutations

The two mutations p.T1173R and p.D253H were deliberately chosen for subsequent functional studies because they were homozygous. Also, since past functional studies of ABCA3 focused mainly on NRD-associated mutations, it was crucial to study the consequences of these two mutations associated with progression towards ILD.

ABCA3 localization and processing. We first investigated the intracellular localization of the mutated ABCA3 protein.

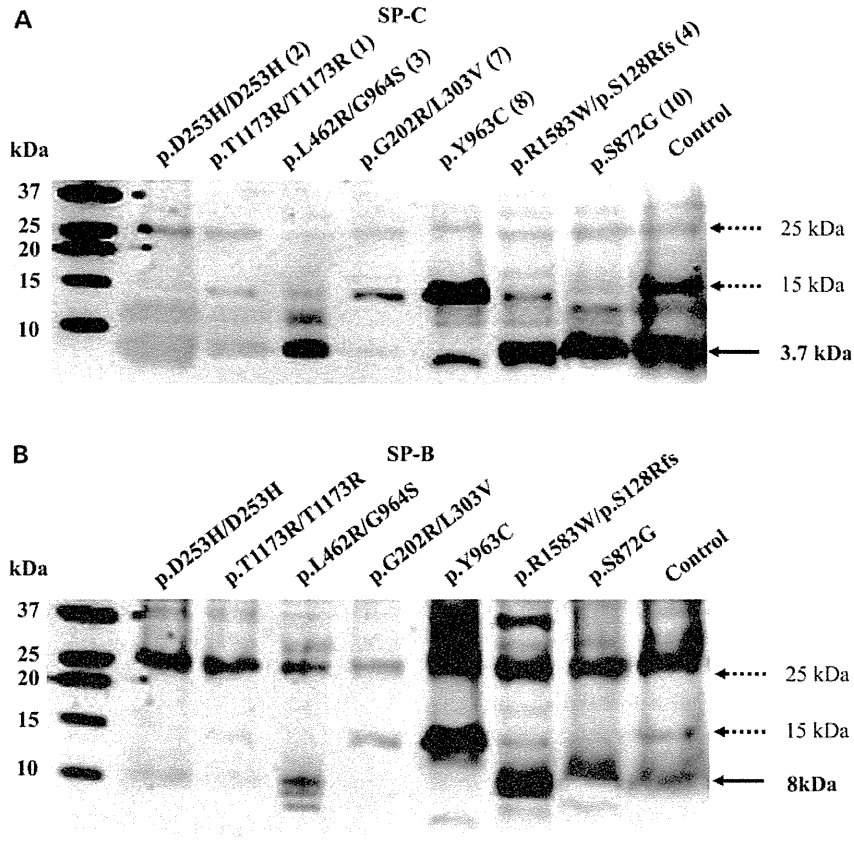

Figure 4. Western blot analysis of surfactant proteins B and C (SP-B and SP-C, respectively) in BALF from seven patients with *ABCA3* mutations and from a control without ILD. Dashed arrows indicate proSP-C (15 and 25 kDa) and proSP-B (15 and 25 kDa). Plain arrows indicate mature SP-C (3.7 kDa) and SP-B (8 kDa).

Similar to the WT protein, ABCA3 mutants co-localized with Lysotracker staining and partially with ERtracker staining (Fig. 5). ABCA3 might co-localize with ER during their folding. However, no accumulation in the ER was observed. The same results were obtained with transiently transfected cells (data not shown). Thus, p.D253H and p.T1173R mutants were not associated with a localization defect. ABCA3 expression was studied on protein extracts from A549-transfected cells. In WT, p.T1173R and p.D253H cells, anti-GFP antibody revealed two bands of 180 kDa (150 kDa ABCA3 + 30 kDa GFP) and 220 kDa (190 + 30 kDa GFP), respectively (Fig. 6). As previously suggested, these two bands might reflect two processing forms (15–18).

Lamellar bodies in ABCA3 WT, p.D253H and p.T1173R cells. Lamellar bodies were not observed in A549 cells (Fig. 7). As shown previously with HEK293 cells (15), transfection of ABCA3 in A549 cells is sufficient to induce lamellar body formation (Fig. 7). The p.D253H mutation induced abnormal lamellar bodies with electron-dense inclusions (Fig. 7, dashed arrows), consistent with the results of the patient's lung biopsy (Fig. 3C). In cells transfected with the p.T1173R mutation, abnormal lamellar bodies are the most frequently observed (irregularly arranged, phospholipid lamellae but eccentrically packed), even if some appeared almost normal.

Cytokine production by ABCA3 WT, p.D253H and p.T1173R cells. We next investigated whether ABCA3 mutants could induce inflammation. IL-8 was chosen as a well-known marker in inflammatory chronic lung disease. Using quantitative PCR (qPCR), we found that IL-8 mRNA levels were increased in p.T1173R cells (Fig. 8A). A significant, faint increase in IL-8 mRNA expression was also observed between WT and p.D253H cells. ABCA3 mRNA levels were similar in WT and mutated cells (data not shown), indicating that the increased IL-8 mRNA level in p.T1173R cells was not due to a transfection issue. At the protein level, ELISA results confirmed that A549 cells expressing the p.T1173R mutant produced more IL-8 than did WT cells (Fig. 8A). In contrast, IL-8 production by p.D253H cells was similar to that of WT cells (Fig. 8B). Finally, TGF-β and MCP-1secretions were similar between WT and transfected cells (data not shown).

IL-8 production is controlled chiefly by MAPK and NF-κB signaling (19). To determine whether these signaling pathways were involved in the observed IL-8 overproduction by p.T1173R cells, we used specific inhibitors. Treatment of cells with inhibitors of MAPK (p38, JNK, ERK1/2) and NF-κB showed that IL-8 production (in WT and mutant cells) was mainly ERK1/2 dependent. The lack of involvement of NF-κB was confirmed by measuring NF-κB promoter activity as done previously (20) (data not shown). However, with

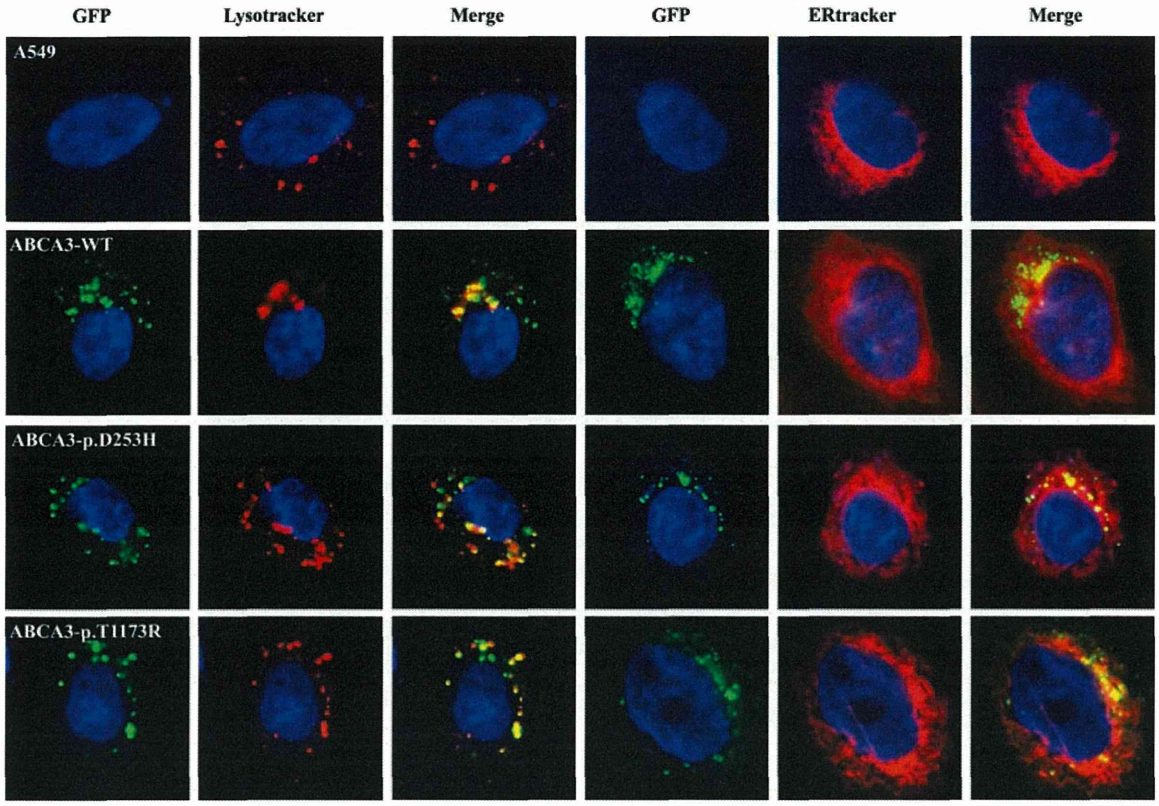

Figure 5. Intracellular localization of wild-type ABCA3 and of the p.D253H and p.T1173R mutants. A549 cells either non-transfected or transfected with mock vector, wild-type protein ABCA3-WT (**A**) or mutated proteins p.D253H (**B**) and p.T1173R (**C**) were analyzed using confocal microscopy. Lysotracker and ERtracker were used to stain lysosomes and the endoplasmic reticulum, respectively.

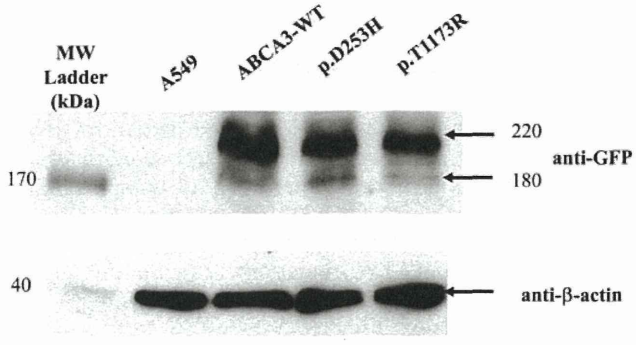

Figure 6. Western blot analysis of ABCA3 in cells transiently transfected with ABCA3-WT or the p.D253H or p.T1173R mutation. ABCA3 expression was detected using anti-GFP antibody (top panel). Equal loading was verified using anti-β actin antibody (bottom panel).

ERK1/2 inhibitor treatment, IL-8 production by p.T1173R cells remained increased compared with WT and p.D253H cells. These results suggest that, even if ERK1/2 signaling is involved in IL-8 production, another signaling pathway may be involved in the increased IL-8 production detected in p.T1173R cells.

Western blot and relative quantification of ERK1/2 phosphorylation confirmed that the observed IL-8 overproduction in p.T1173R cells was independent of ERK1/2 signaling. Finally, caspase 3/7 activity was similar in WT and mutant cells, indicating that these mutations did not induce apoptosis.

DISCUSSION

We identified 15 (13 novel) *ABCA3* mutations in 47 children (32%) who had NRD and/or ILD and no *SFTPB* or *SFTPC* mutations (5). None of these mutations was found in either the public polymorphism database or our controls. The amino acids affected by the mutations were conserved in mammalian *ABCA3* sequences. All 10 patients with *ABCA3* (21%) mutations had severe respiratory symptoms and abnormal chest imaging findings. Ninety percent of patients harboring *ABCA3* mutations had NRD. Finally, parents heterozygous for the p.R1583W, p.S128Rfs, p.R1521W or p.R208V mutations were not affected. In three patients, a mutation was found in a single allele but the clinical phenotype (NRD) may support the existence of a second mutation (in introns, deletions and so on) not detected by our sequencing method. Haploinsufficiency has been suggested as a mechanism leading to clinical phenotype emergence in patients with only one mutated allele (10,21). Similarly, *Abca3*$^{+/-}$ mice, despite normal respiratory function, had fewer lamellar bodies and altered surfactant lipid synthesis compared with wild-type mice, suggesting susceptibility to NRD or ILD (22). However, even if the observed clinical phenotypes are

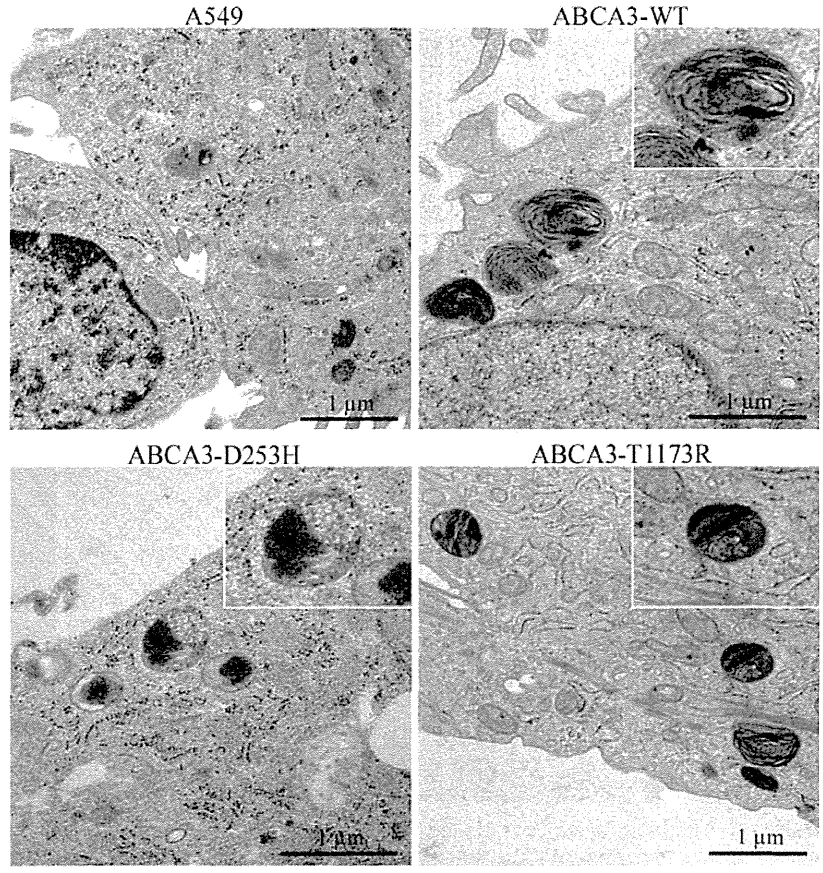

Figure 7. Lamellar body analysis. A549 cells transfected with mock vector (pEGFP-N1), ABCA3-WT (**A**), or mutated ABCA3-D253H (**B**) or ABCA3-T1173R-GFP were analyzed using electron microscopy.

compatible with *ABCA3* deficiency, we cannot conclude that *ABCA3* heterozygosis is responsible for this phenotype.

As previously described (1,11,13), some patients with *ABCA3* mutations had a less severe phenotype than that usually associated with *ABCA3* mutations (10). These variations in the clinical and radiological features may be related to the nature of the mutation (16). Previous studies showed that *ABCA3* mutations led to abnormal processing and/or trafficking of the ABCA3 protein (15), alterations in ABCA3 protein functions such as ATPase activity (16), or impaired lipid transport (23). Interactions with variants in other genes and/or with external factors such as viral infections may also influence the observed phenotype (24).

ABCA3 deficiency in full-term patients with NRD was shown previously to be associated with abnormal processing of SP-B and SP-C with an accumulation of precursors of SP-B and absence of mature SP-C (11). In our patients with *ABCA3* deficiency, we observed that SP-C and SP-B expression levels varied considerably across patients. Indeed, less severe patients had decreased amounts of SP-B and SP-C, whereas patient who died of respiratory failure showed normal expression of both proteins. This discrepancy may be explained by our technique of western blot, which is performed on lyophilized supernatant and improved the level of surfactant protein detection. It may also be explained by the function of ABCA3, which is critical for the proper formation of lamellar bodies and surfactant function but is not responsible for SP-B or SP-C synthesis. Hence, the pattern of SPs may be independent of the clinical status. To confirm the hypothesis, it would have been interesting to compare the patterns of siblings harboring the p.D253H mutation. Unfortunately, BALF from this patient was not available. Finally, as reported previously for *SFTPC* mutations (25), the presence or absence of SP-B and SP-C might be neither sensitive nor specific for *ABCA3*-related diseases.

Electron microscopy examination of a lung biopsy specimen is the reference standard for evaluating lamellar body characteristics and for providing a preliminary diagnosis prior to *ABCA3* gene analysis. Indeed, abnormal lamellar bodies with electron-dense inclusions have been described in association with *ABCA3* mutations in previous studies (10,21,26). However, electron microscopy cannot be performed routinely. The presence of abnormal lamellar bodies in the patient harboring the p.D253H mutation supports a pathogenic effect of this mutation. These abnormalities were also observed *in vitro* in p.D253H- and p.T1173R-transfected cells, suggesting that *ABCA3* abnormalities may consistently induce abnormal lamellar bodies. However, since we do not have the corresponding biopsy from the patient harboring the p.T1173R, we cannot draw a firm conclusion on this point.

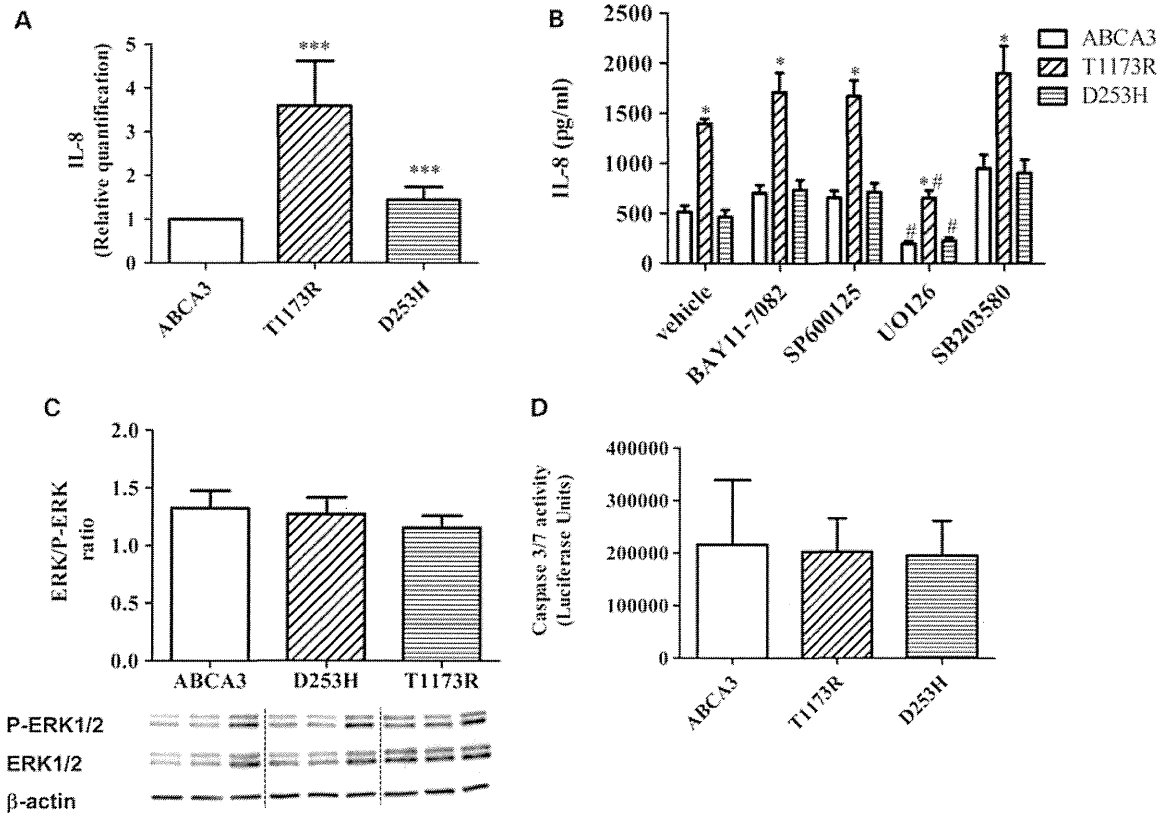

Figure 8. (**A**) IL-8 mRNA relative quantification was performed using qPCR. Results are representative of the mean ± SD of three experiments performed in triplicate. $^{***}P \leq 0.001$. (**B**) Role for MAPK and NF-κB-dependent signaling in IL-8 secretion by ABCA3-WT, D253H and T1173R cells. Cells were treated with 10 μM inhibitors of ERK1/2 (U0126), p38 (SB203580), JNK (SP600125) or NF-κB (BAY11-7082) for 24 h; $^{*}P \leq 0.05$: ABCA3 versus T1173R; $\#P \leq 0.05$: vehicle versus U0126. Supernatants were tested for IL-8 by ELISA. Data are means ± SD of three experiments performed in triplicate. (**C**) ERK1/2 phosphorylation measurement. Data are means ± SD of four experiments performed in triplicate. Results are expressed as P-ERK/ERK ratio (top panel). Western blot analysis of phospho-ERK1/2, total ERK1/2 and β-actin (bottom panel). (**D**) Caspase 3/7 activity. Data are means ± SD of three experiments performed in triplicate.

We performed *in vitro* experiments to elucidate the pathophysiological effects of two mutations associated with progression towards ILD, p.D253H and T1173R. These mutations did not alter the localization or maturation of the protein. Past functional studies on other *ABCA3* mutations showed localization/folding defects or functional defects (15,16,18,21,23,27). As pointed out recently, the effect of *ABCA3* mutations on lung epithelial cells depends on the ABCA3 protein defects (18). We found that the functional abnormalities differed between the two mutations. The p.D253H and p.T1173R mutations induced abnormal lamellar bodies. ABCA3 being a major transporter of phosphatidylcholine and phosphatidylglycerol into lamellar bodies, the lamellar body alterations suggest abnormalities in phospholipid trafficking that need to be characterized. The recent proteomic characterization of lamellar bodies may help to achieve this challenging objective (28). The p.T1173R mutation was also associated with increased production of IL-8, a well-known chemotactic molecule for neutrophils. Interestingly, increased IL-8 production was also detected in cells expressing *SFTPC* (Δexon 4 and the common p.I73T) mutations (29). In contrast, we do not find differences in TGF-β production, a cytokine that has been extensively studied in adults with idiopathic pulmonary fibrosis (30). Also, no differences in MCP-1 production were observed between WT and mutated cells. MCP-1 has been shown previously to contribute to the pathogenesis of pediatric ILD (31). However, in this study, none of the children had familial ILD, and surfactant genetic screening was not done, thus we do not know whether MCP-1 production is related to surfactant-associated disorders. In fact, surfactant genetic disorders are a subclass of pediatric ILD (2), which include various clinical phenotypes associated with specific clinical and biological features. Altered intercellular signaling was also shown recently in cells expressing *SFTPC* variants. CXCR1 and CCR2 expression by lymphocytes and neutrophils is probably dependent on an unidentified soluble mediator secreted by p.I73T cells (32). These studies, combined with our data, suggest that inflammatory pathways are involved in genetic surfactant disorders. However, better characterization of these pathways is required if specific treatments are to be sought.

In conclusion, although rare, ABCA3 deficiency should be considered in full-term newborns with severe respiratory distress and in older patients with ILD. Since *ABCA3* mutations lead to distinct functional defects, functional analysis of each *ABCA3* mutation is necessary to identify specific molecular targets that could be modulated or corrected by therapeutic agents.

MATERIALS AND METHODS

Patients

Through a national program on rare lung diseases, which has been described elsewhere (5), we recruited 121 pediatric patients with diffuse lung disease, over a 5-year period (2002–2007). Among the 121 patients with diffuse lung disease, 86 had respiratory distress, 59 presenting with neonatal onset (NRD) and 18 patients died. *ABCA3* genetic screening was performed in 47 children with severe respiratory distress or familial history compatible with autosomal recessive inheritance. Patients with presence of *SFTPC* or *SFTPB* mutations or insufficient information from medical records were excluded.

For each patient, we retrieved the following information from the medical records: family history, clinical presentation, findings by radiography and HRCT of the chest and lung biopsy findings (including those obtained by electron microscopy). The control for the BALF study was one child with uveitis who underwent bronchoscopy because of suspected sarcoidosis. Bronchoscopy showed no evidence of sarcoidosis or ILD. The control population for the genetic tests consisted of 23 individuals of European descent who had no history of lung disease. The protocol was accepted by the appropriate Committee for the Protection of Individuals in Biochemical Research, as required by French legislation. Written informed consent was obtained from the patients or their next of kin before study inclusion (5).

Genetic analysis

Genomic DNA was extracted from blood samples using an automated BioRobot EZ1 workstation (Qiagen, Hilden, Germany). Parental DNA was sequenced when samples were available. *ABCA3* primers were designed to amplify the 30 coding exons and their respective splice junctions (10). Primers were purchased from Sigma-Aldrich (Lyon, France) and Taq polymerase from Applied Biosystems (Foster City, CA, USA). Sequencing reactions were performed as described previously (5). Identified mutations were verified on two PCR products. Nucleotide numbering reflected *ABCA3* cDNA numbering, with +1 corresponding to the A of the ATG translation initiation codon in the reference sequence NM_001089.2. The reference sequence NP_001080.2 of ABCA3 protein was used for amino acid numbering.

Histological examination of lung tissue

Lung tissue obtained by surgical biopsy was examined by light microscopy using a standard hematoxylin and eosin staining protocol. Electron microscopy was conducted using standard protocols.

Collection of BALF

We retrospectively analyzed BALF from seven children with *ABCA3* mutations. Fiber-optic bronchoscopy with bronchoalveolar lavage was performed under sedation, as previously described (33).

ABCA3 vectors

The pEGFPN1-ABCA3 plasmid, called ABCA3-WT hereafter, was obtained as described previously (16). Mutagenesis was induced using PCR-based site-directed mutagenesis (QuikChange Site-Directed Mutagenesis Kit, Stratagene, La Jolla, CA, USA). Mutagenesis primers (Sigma) were as follows: *D253H-For*-5′-ACCCGCCGTTCATCGCACACCCCTTCC-3′, *D253H-Rev*-5′-GGAAGGGGTGTGCGATGAACGGCGGGT-3′; *T1173R-For*-5′-ACGTGCGTGCCTTCAGGCGGGACG-3′, and *T1173R-Rev*-5′-CGTCCCGCCTGAAGGCACGCACGT-3′. Mutagenesis was confirmed by sequencing.

Cell culture and transfection

A549 cells were cultured as described previously (34). Cells (1×10^6) were transfected with 1 μg of ABCA3-WT, ABCA3-D253H or ABCA3-T1173R plasmid using a nucleofector device (Lonza, Cologne, Germany) as recommended by the manufacturer. For stable transfection, GFP-positive cells were selected using a FACSAria cell sorter (BD, Le Pont-De-Claix, France) and plated with 0.5 mg/ml of Geneticin (Invitrogen, Paisley, UK). Three weeks after selection, stably transfected cells were examined by immunofluorescence and maintained with 0.3 mg/ml of Geneticin. Experiments with transiently transfected cells (Lipofectamine, Invitrogen) were performed 24 h post-transfection. Analysis of NF-κB activation was done with NF-κB luciferase plasmid (20).

Fluorescence microscopy

Cells transfected transiently or stably with A549 were plated in 35 mm Petri dishes (iBidi, Martinsried, Germany). Living cells were stained with either Lysotracker red (lysosome probe) or ERtracker red (endoplasmic reticulum probe) (Invitrogen, Paisley, UK). DAPI (Sigma-Aldrich, Lyon, France) was used to stain the nucleus. Fluorescence microscopy was achieved using a Zeiss Axiovert 200 microscope (Zeiss, Le Pecq, France).

Cytokine/ERK ELISA and caspase 3/7

Cells stably transfected with A549 (1×10^5) were seeded in 96-well plates (TPP, Trasadingen, Switzerland). After 24 h, the cells were incubated with vehicle (DMSO) or 10 μM inhibitors of ERK1/2 (U0126), p38 (SB203580), JNK (SP600125) (Sigma-Aldrich) or NF-κB (BAY11-7082) (Calbiochem, San Diego, CA, USA). Human IL-8, MCP-1 and TGF-β concentrations in cell culture supernatants were determined 24 h later using the DuoSet enzyme-linked immunosorbent assay kit (R&D Systems, Minneapolis, MN, USA). Relative ERK1/2 phosphorylation was measured using a cell-based ERK1/2 ELISA kit (RayBiotech, Norcross, GA, USA) following the manufacturer's instructions. Caspase 3/7 activity (Promega, Madison, WI, USA) was measured as recommended by the manufacturer.

IL8 real-time qPCR

Total RNA was extracted using a nucleospin extract II kit (Macherey Nagel, Duren, Germany). Reverse transcription was performed with 0.8 μg of total extracted RNA, using the ABI high-capacity cDNA archive kit (Applied Biosystems). RT-PCR was performed using an ABI StepOnePlus™. Each reaction contained 10 μl of 2× TaqMan® Fast Universal PCR Master Mix (Applied Biosystems), 1 μl of IL-8 (Hs00174103_m1), ABCA3 (Hs00975518_m1) or GAPDH (Hs03929097_g1) TaqMan® probe and 40 ng of cDNA as the template in a final volume of 20 μl. Data were analyzed using the comparative C_t method ($\Delta\Delta C_t$). For relative quantification, the amount of IL-8 was normalized for GAPDH (endogenous gene) relative to wild-type cells (ABCA3-WT) used as the calibrator and was calculated using the $2^{-\Delta\Delta C}t$method as published previously (35). Each point corresponds to the mean ± SD of three experiments performed in triplicate.

Western blot

BALF proteins were accurately quantified using a Qubit fluorometer (Invitrogen). Then, 24 μg of protein was fractionated using SDS–PAGE on 16% Tris–tricine gels, electrotransferred and probed by immunoblotting using antibodies to surfactant proteins SP-B and SP-C (Seven Hills Bioreagents, Cincinnati, OH, USA), as described previously (33).

A549 cell extracts were prepared from 3×10^5 cells and solubilized as described previously (34). An equal amount of protein (10 μg) from each sample was size-separated on 10% SDS–polyacrylamide gel and electrotransferred to a nitrocellulose membrane (Bio-Rad, Hercules, CA, USA). Immunodetection was performed with antibodies specific for the total and phosphorylated forms of ERK1/2 (Cell Signaling Technology, Beverly, MA, USA) and β-actin (Sigma-Aldrich). Secondary antibodies were from Cell Signaling Technology. Bound antibodies were detected using Super-Signal West Femto chemiluminescent substrate (Pierce, Rockford, IL, USA) according to the manufacturer's instructions. Between successive probes, membranes were treated with Restore Western Blot Stripping Reagent (Pierce). Molecular masses were determined using the SeeBlue® Plus2 Pre-Stained Standard (Invitrogen). Images were recorded with a Fujifilm LAS-3000 bioimaging system (Fujifilm, Stamford, CT, USA).

For the study of ABCA3 expression, 35 μg of transiently transfected cells (Lipofectamin, 48 h) was used. Immunoblotting was performed with an anti-eGFP antibody (Clontech, Mountain View, CA, USA).

Statistics

The statistical significance of differences between groups was tested using the unpaired Student's *t*-test with a threshold of $P < 0.05$.

SUPPLEMENTARY MATERIAL

Supplementary Material is available at *HMG* online.

ACKNOWLEDGEMENTS

We thank the patients and their families for their cooperation in this study. We are grateful to Marie-Claude Miesch, Catherine Meunier, France Michel, Corinne Chauve, Isabelle Sargis and Magali Niasme for their expert technical assistance. We thank Professor M. Griese and Dr R. Zarbock for assistance with ABCA3 western blotting. We thank A. Wolfe for assistance in improving the manuscript.

Conflict of Interest statement. None declared.

FUNDING

This work was supported by a Legs Poix (Chancelleries des Universités de Paris, to L.G.), the Assistance Publique-Hôpitaux de Paris [Surfactant Disorders and Chronic Lung Disease (APSE), ClinicalTrials.gov #NCT00783978, to R.E.] and from the United States National Institutes of Health (HL54703 to L.M.N.). F.F. was supported by a PhD fellowship from the SPLF (Société de Pneumologie de Langue Française).

REFERENCES

1. Bullard, J.E., Wert, S.E., Whitsett, J.A., Dean, M. and Nogee, L.M. (2005) ABCA3 mutations associated with pediatric interstitial lung disease. *Am. J. Respir. Crit. Care. Med.*, **172**, 1026–1031.
2. Deutsch, G.H., Young, L.R., Deterding, R.R., Fan, L.L., Dell, S.D., Bean, J.A., Brody, A.S., Nogee, L.M., Trapnell, B.C., Langston, C. *et al.* (2007) Diffuse lung disease in young children: application of a novel classification scheme. *Am. J. Respir. Crit. Care. Med.*, **176**, 1120–1128.
3. Hartl, D. and Griese, M. (2005) Interstitial lung disease in children—genetic background and associated phenotypes. *Respir. Res.*, **6**, 32.
4. Nogee, L.M., Garnier, G., Dietz, H.C., Singer, L., Murphy, A.M., deMello, D.E. and Colten, H.R. (1994) A mutation in the surfactant protein B gene responsible for fatal neonatal respiratory disease in multiple kindreds. *J. Clin. Invest.*, **93**, 1860–1863.
5. Guillot, L., Epaud, R., Thouvenin, G., Jonard, L., Mohsni, A., Couderc, R., Counil, F., de Blic, J., Taam, R.A., Le Bourgeois, M. *et al.* (2009) New surfactant protein C gene mutations associated with diffuse lung disease. *J. Med. Genet.*, **46**, 490–494.
6. Stahlman, M.T., Besnard, V., Wert, S.E., Weaver, T.E., Dingle, S., Xu, Y., von Zychlin, K., Olson, S.J. and Whitsett, J.A. (2007) Expression of ABCA3 in developing lung and other tissues. *J. Histochem. Cytochem.*, **55**, 71–83.
7. Mulugeta, S., Gray, J.M., Notarfrancesco, K.L., Gonzales, L.W., Koval, M., Feinstein, S.I., Ballard, P.L., Fisher, A.B. and Shuman, H. (2002) Identification of LBM180, a lamellar body limiting membrane protein of alveolar type II cells, as the ABC transporter protein ABCA3. *J. Biol. Chem.*, **277**, 22147–22155.
8. Connors, T.D., Van Raay, T.J., Petry, L.R., Klinger, K.W., Landes, G.M. and Burn, T.C. (1997) The cloning of a human ABC gene (ABC3) mapping to chromosome 16p13.3. *Genomics*, **39**, 231–234.
9. Klugbauer, N. and Hofmann, F. (1996) Primary structure of a novel ABC transporter with a chromosomal localization on the band encoding the multidrug resistance-associated protein. *FEBS Lett.*, **391**, 61–65.
10. Shulenin, S., Nogee, L.M., Annilo, T., Wert, S.E., Whitsett, J.A. and Dean, M. (2004) ABCA3 gene mutations in newborns with fatal surfactant deficiency. *N. Engl. J. Med.*, **350**, 1296–1303.
11. Brasch, F., Schimanski, S., Muhlfeld, C., Barlage, S., Langmann, T., Aslanidis, C., Boettcher, A., Dada, A., Schroten, H., Mildenberger, E. *et al.* (2006) Alteration of the pulmonary surfactant system in full-term infants with hereditary ABCA3 deficiency. *Am. J. Respir. Crit. Care. Med.*, **174**, 571–580.
12. Whitsett, J.A., Wert, S.E. and Xu, Y. (2005) Genetic disorders of surfactant homeostasis. *Biol. Neonate.*, **87**, 283–287.
13. Doan, M.L., Guillerman, R.P., Dishop, M.K., Nogee, L.M., Langston, C., Mallory, G.B., Sockrider, M.M. and Fan, L.L. (2008) Clinical,

radiological and pathological features of ABCA3 mutations in children. *Thorax*, **63**, 366–373.
14. Somaschini, M., Nogee, L.M., Sassi, I., Danhaive, O., Presi, S., Boldrini, R., Montrasio, C., Ferrari, M., Wert, S.E. and Carrera, P. (2007) Unexplained neonatal respiratory distress due to congenital surfactant deficiency. *J. Pediatr.*, **150**, 649–653, 653 e641.
15. Cheong, N., Madesh, M., Gonzales, L.W., Zhao, M., Yu, K., Ballard, P.L. and Shuman, H. (2006) Functional and trafficking defects in ATP binding cassette A3 mutants associated with respiratory distress syndrome. *J. Biol. Chem.*, **281**, 9791–9800.
16. Matsumura, Y., Ban, N., Ueda, K. and Inagaki, N. (2006) Characterization and classification of ATP-binding cassette transporter ABCA3 mutants in fatal surfactant deficiency. *J. Biol. Chem.*, **281**, 34503–34514.
17. Nagata, K., Yamamoto, A., Ban, N., Tanaka, A.R., Matsuo, M., Kioka, N., Inagaki, N. and Ueda, K. (2004) Human ABCA3, a product of a responsible gene for abca3 for fatal surfactant deficiency in newborns, exhibits unique ATP hydrolysis activity and generates intracellular multilamellar vesicles. *Biochem. Biophys. Res. Commun.*, **324**, 262–268.
18. Weichert, N., Kaltenborn, E., Hector, A., Woischnik, M., Schams, A., Holzinger, A., Kern, S. and Griese, M. (2011) Some ABCA3 mutations elevate ER stress and initiate apoptosis of lung epithelial cells. *Respir. Res.*, **12**, 4.
19. Hoffmann, E., Dittrich-Breiholz, O., Holtmann, H. and Kracht, M. (2002) Multiple control of interleukin-8 gene expression. *J. Leukoc. Biol.*, **72**, 847–855.
20. Muselet-Charlier, C., Roque, T., Boncoeur, E., Chadelat, K., Clement, A., Jacquot, J. and Tabary, O. (2007) Enhanced IL-1beta-induced IL-8 production in cystic fibrosis lung epithelial cells is dependent of both mitogen-activated protein kinases and NF-kappaB signaling. *Biochem. Biophys. Res. Commun.*, **357**, 402–407.
21. Park, S.K., Amos, L., Rao, A., Quasney, M.W., Matsumura, Y., Inagaki, N. and Dahmer, M.K. (2010) Identification and characterization of a novel ABCA3 mutation. *Physiol. Genomics*, **40**, 94–99.
22. Cheong, N., Zhang, H., Madesh, M., Zhao, M., Yu, K., Dodia, C., Fisher, A.B., Savani, R.C. and Shuman, H. (2007) ABCA3 is critical for lamellar body biogenesis in vivo. *J. Biol. Chem.*, **282**, 23811–23817.
23. Matsumura, Y., Ban, N. and Inagaki, N. (2008) Aberrant catalytic cycle and impaired lipid transport into intracellular vesicles in ABCA3 mutants associated with nonfatal pediatric interstitial lung disease. *Am. J. Physiol. Lung Cell. Mol. Physiol.*, **295**, L698–707.
24. Bullard, J.E. and Nogee, L.M. (2007) Heterozygosity for ABCA3 mutations modifies the severity of lung disease associated with a surfactant protein C gene (SFTPC) mutation. *Pediatr. Res.*, **62**, 176–179.
25. Hamvas, A. (2006) Inherited surfactant protein-B deficiency and surfactant protein-C associated disease: clinical features and evaluation. *Semin. Perinatol.*, **30**, 316–326.
26. Edwards, V., Cutz, E., Viero, S., Moore, A.M. and Nogee, L. (2005) Ultrastructure of lamellar bodies in congenital surfactant deficiency. *Ultrastruct. Pathol.*, **29**, 503–509.
27. Matsumura, Y., Sakai, H., Sasaki, M., Ban, N. and Inagaki, N. (2007) ABCA3-mediated choline-phospholipids uptake into intracellular vesicles in A549 cells. *FEBS Lett.*, **581**, 3139–3144.
28. Ridsdale, R., Na, C.L., Xu, Y., Greis, K.D. and Weaver, T. (2010) Comparative proteomic analysis of lung lamellar bodies and lysosome-related organelles. *PLoS One*, **6**, e16482.
29. Maguire, J.A., Mulugeta, S. and Beers, M.F. (2011) Endoplasmic reticulum stress induced by surfactant protein C BRICHOS mutants promotes proinflammatory signaling by epithelial cells. *Am. J. Respir. Cell Mol. Biol.*, **44**, 404–414.
30. Willis, B.C. and Borok, Z. (2007) TGF-beta-induced EMT: mechanisms and implications for fibrotic lung disease. *Am. J. Physiol. Lung Cell. Mol. Physiol.*, **293**, L525–534.
31. Hartl, D., Griese, M., Nicolai, T., Zissel, G., Prell, C., Reinhardt, D., Schendel, D.J. and Krauss-Etschmann, S. (2005) A role for MCP-1/CCR2 in interstitial lung disease in children. *Respir. Res.*, **6**, 93.
32. Woischnik, M., Sparr, C., Kern, S., Thurm, T., Hector, A., Hartl, D., Liebisch, G., Mulugeta, S., Beers, M.F., Schmitz, G. *et al.* (2010) A non-BRICHOS surfactant protein c mutation disrupts epithelial cell function and intercellular signaling. *BMC Cell Biol.*, **11**, 88.
33. Guillot, L., Carre, A., Szinnai, G., Castanet, M., Tron, E., Jaubert, F., Broutin, I., Counil, F., Feldmann, D., Clement, A. *et al.* (2010) NKX2-1 mutations leading to surfactant protein promoter dysregulation cause interstitial lung disease in 'brain-lung-thyroid syndrome'. *Hum. Mutat.*, **31**, E1146–E1162.
34. Guillot, L., Medjane, S., Le-Barillec, K., Balloy, V., Danel, C., Chignard, M. and Si-Tahar, M. (2004) Response of human pulmonary epithelial cells to lipopolysaccharide involves Toll-like receptor 4 (TLR4)-dependent signaling pathways: evidence for an intracellular compartmentalization of TLR4. *J. Biol. Chem.*, **279**, 2712–2718.
35. Guillot, L., Carroll, S.F., Badawy, M. and Qureshi, S.T. (2008) Cryptococcus neoformans induces IL-8 secretion and CXCL1 expression by human bronchial epithelial cells. *Respir. Res.*, **9**, 9.

ORIGINAL ARTICLE

Sorting nexin 19 regulates the number of dense core vesicles in pancreatic β-cells

Shin-ichi Harashima[1]*, Takahiko Horiuchi[2], Yu Wang[1], Abner Louis Notkins[3], Yutaka Seino[1], Nobuya Inagaki[1]

ABSTRACT

Aims/Introduction: Insulinoma-associated protein 2 (IA-2) regulates insulin secretion and the number of dense core vesicles (DCV). However, the mechanism of regulation of DCV number by IA-2 is unknown. We examined the effect of sorting nexin 19 (SNX19), an IA-2 interacting protein, on insulin secretion and the number of dense core vesicles (DCV).

Materials and Methods: Stable SNX19 knockdown (SNX19KD) MIN6, a mouse pancreatic β-cell line, and stable SNX19-reintroduced SNX19KD MIN6 were established. Quantification of DCV, and lysosomes was carried out using electron micrographs. The half-life of DCV was detected by pulse-chase experiment.

Results: Insulin secretion and content were decreased in stable SNX19KD MIN6 cells compared with those in control MIN6 cells. Electron micrographs showed that DCV number in SNX19KD cells was decreased by approximately 75% and that DCV size was decreased by approximately 40% compared with those in control cells, respectively. Furthermore, when SNX19 was reintroduced in SNX19KD cells, insulin content, insulin secretion and DCV number were increased. The half-life of DCV was decreased in SNX19KD cells, but was increased in SNX19KD cells in which SNX19 was reintroduced. The number of lysosomes and the activity of lysosome enzyme cathepsin D were increased by approximately threefold in SNX19KD cells compared with those in control cells. In contrast, they were decreased to approximately half to one-third in SNX19-reintroduced SNX19KD cells.

Conclusions: SNX19 regulates the number of DCV and insulin content by stabilizing DCV in β-cells. (J Diabetes Invest, doi: 10.1111/j.2040-1124.2011.00138.x, 2012)

KEY WORDS: Sorting nexin 19, Insulinoma-associated protein 2, Dense core vesicles

INTRODUCTION

The sorting nexins (SNX) belong to a large family involved in protein sorting and intracellular trafficking[1,2]. SNX19 is a 992 amino acid member of this family that has a phox (PX) domain (a binding motif to phosphatidylinositol) at the COOH-terminus and a PX-associated (PXA) domain at the NH2-terminus[3,4]. The function of SNX19 is not known, but it binds to the dense core vesicle (DCV) transmembrane protein insulinoma-associated protein 2 (IA-2)[5].

IA-2 is a major autoantigen in type 1 diabetes[6,7], and autoantibodies to it are found in 70–80% of newly diagnosed patients. These autoantibodies appear years before the onset of clinical disease, and individuals with autoantibodies to both IA-2 and GAD65 have approximately a 50% risk of developing type 1 diabetes within 5 years. Based on sequence, IA-2 is a member of the protein tyrosine phosphate (PTP) family, but because of two amino acid substitutions in the PTP domain, it is enzymatically inactive with conventional PTP substrates[8]. IA-2 is present in neuroendocrine cells throughout the body and knockout of IA-2 in mice results in impaired secretion of hormones and neurotransmitters, and a variety of phenotypes characterized by impaired insulin secretion, glucose intolerance[9,10], female infertility[11], abnormalities in learning and behavior[12], and loss of circadian rhythm[13]. Overexpression of IA-2 in MIN6 cells and rat pheochromocytoma cell line PC12 cells increased insulin secretion[14] and dopamine release[15], respectively.

Because SNX19 binds to IA-2, the present experiments were initiated to study the effects of knockdown and reconstitution of SNX19 in MIN6 cells on the biology and physiology of DCV, including their half-life, and number and the cellular content and secretion of insulin. We show here that SNX19 regulates the DCV number and insulin content by modulating the half-life of DCV in pancreatic β-cells.

MATERIALS AND METHODS

Reagents

pCMV-Tag3 mammalian expression vectors with G418 resistance gene were purchased from Agilent technologies (Santa Clara, CA, USA), pSilencer3.1-CMV hygro mammalian siRNA expression vector from Applied Biosystem (Austin, TX, USA), Effectene transfection reagent from Qiagen (Santa Clarita, CA, USA), mouse IA-2 antibody from LAD (Berlin, Germany), mouse anti-α-tubulin antibody from Sigma (St. Louis, MO,

[1]Department of Diabetes and Clinical Nutrition, Graduate School of Medicine, Kyoto University, Kyoto, [2]Department of Medicine and Biosystemic Science, Graduate School of Medical Sciences, Kyushu University, Fukuoka, Japan, and [3]Experimental Medicine Section, Oral Infection and Immunity Branch, National Institute of Dental and Craniofacial Research (NIDCR), National Institutes of Health (NIH), Bethesda, MD, USA
*Corresponding author. Shin-ichi Harashima Tel.: +81-75-751-3560
Fax: +81-75-771-6601 E-mail address: harasima@metab.kuhp.kyoto-u.ac.jp
Received 22 March 2011; revised 12 April 2011; accepted 2 May 2011

USA), anti-SNX19 antibody from Santa Cruz biotechnology (Santa Cruz, CA, USA) and mouse insulin ELISA kit from Shibayagi (Shibukawa, Japan).

Plasmids

Two SNX19 siRNA were synthesized by Takara (Otsu, Japan); the sequences were 5′-AATTGCACCTGGAACGATTCA-3′ and 5′-AAAGGCAGCTGGAACAGGAGA-3′, and were inserted into pSilencer 3.1-CMV hygro vector. Primers for complementary SNX19 were synthesized by Takara. The forward and reverse primer sequences for SNX19 were 5′-CCGCTCGAGATGAAGACAGAAACAGTG-3′ and 5′-CCGCTCGAGCTAAGAGGAGACACCCAT-3′. SNX19 polymerase chain reaction (PCR) product was inserted into pCMV-Tag3 at *Xho*I sites. All plasmids were sequenced and no mutations were found.

Establishment of Stable Cell Lines

MIN6 cells were maintained in Dulbecco's modified Eagle's medium (DMEM) containing 25 mmol/L D-glucose (high glucose), supplemented with 15% heat-inactivated fetal bovine serum, 100 U/mL penicillin and 100 μg/mL streptomycin at 37°C in 95% air and 5% CO_2. SNX19 siRNA inserted into pSilence3.1-CMV hygro vector were introduced into MIN6 cells with Effectene transfection reagent, and stably transfected cells were selected by 200 μg/mL of hygromycin and by limiting dilution. Full length IA-2 and full length SNX19 were inserted into pCMV-Tag3 vectors and introduced into SNX19 knockdown MIN6 cells using Effectene transfection reagent, and stably transfected cells were selected by 300 μg/mL of G418 and 200 μg/mL of hygromycin, and by limiting dilution. SNX19 and IA-2 expression were confirmed by western blot.

Western Blot

Cells were washed twice with PBS, detached from plates with trypsin-EDTA, collected, washed two more times with PBS and then sonicated in lysis buffer. Equivalent amounts of protein were resolved by sodium dodecyl sulfate–polyacrylamide gel electrophoresis on 4–12% acrylamide gels (Invitrogen, Carlsbad, CA, USA) and transferred to polyvinylidene fluoride membranes (Invitrogen), followed by immunoblotting with antibodies to detect respective proteins.

Cell Proliferation Assay

A total of 1.0×10^4 cells/mL were seeded into a 96-well culture late and incubated for 10 days in 25 mmol/L glucose DMEM media. Cell proliferation was measured at indicated times by a bromodeoxyuridine (BrdU) cell proliferation assay kit (Calbiochem, Damstadt, Germany) as previously reported[16].

Insulin Secretion Test

MIN6 cells were seeded in 96-well culture plates at a density of 3.0×10^4 cells per well and cultured for 3 days. The attached cells were washed twice with 3 mmol/L glucose Krebs–Ringer bicarbonate HEPES (KRBH) buffer (124 mmol/L NaCl, 5.6 mmol/L KCl, 2.5 mmol/L $CaCl_2$ and 20 mmol/L HEPES at pH 7.4). The cells were then incubated at 37°C for 60 min in KRBH buffer, washed and incubated again for 60 min in KRBH at 3 mmol/L glucose. Supernatant was collected and insulin release measured by ELISA kit (Shibayagi). The cells then were incubated at 25 mmol/L glucose in KRBH for 60 min and the amount of insulin released measured again.

Insulin Content

Cells were seeded in 24-well culture plates at a density of 1.0×10^5 cells per well and cultured for 3 days at 25 mmol/L glucose. Media then were removed and replaced again with 25 mmol/L glucose. The cells were incubated for 16 h and the insulin content was determined by ELISA.

Electron Microscopy

Cells were cultured in 25 mmol/L glucose for 3 days. The culture media then were replaced with 25 mmol/L glucose containing fresh DMEM media for 16 h. Cells were washed with PBS three times and fixed with 2.5% glutaraldehyde in 0.1 mol/L phosphate buffer, pH 7.4, and used for electron microscopy study.

Quantification of DCV and Lysosomes Per Cytoplasmic Area

Quantification of DCV was carried out as previously reported[14]. Briefly, 15 cells were selected at random and the images were taken at 8 k magnification. The number of DCV/cytoplasmic area or lysosome/cytoplasmic area was quantified by two operators blind to their status using national Institutes of Health images. Approximately 20 cytoplasmic areas taken by electron microscopy were estimated.

Half-life of DCV

Insulin half-life was determined as previously described[14]. Cells were seeded in 6-well culture plates and incubated for 2 days in 25 mmol/L glucose to obtain a steady state. The cells were then washed with KRBH buffer and incubated in 25 mmol/L glucose luecine-free media with [^{3}H]leucine (Amersham Biosciences, Piscataway, NJ, USA) for 24 h. The media then was changed to 3 mmol/L low glucose without [^{3}H]leucine for a 48 h chase. The cells and supernatant were collected at different times and the cells were lysed by repeated freezing and thawing. The cell lysates and supernatants were incubated at 4°C for 2 h in the presence of anti-insulin or anti-proinsulin antibodies. Antibody-antigen complexes then were precipitated by adding 5 mg of protein A-Sepharose in 100 μL of glycine/BSA/NP-40 buffer. After mixing at 4°C for 2 h, the immunoreactive material bound to the protein A-Sepharose was separated from unbound material in the supernatant by centrifugation (8000 *g*, 30 s). After washing the precipitates twice with 250 μL of glycine/BSA/NP-40, the precipitants were suspended in 250 μL of 1 mol/L acetic acid and 2.5 mg/mL of BSA. The suspended precipitates were added to liquid scintillation vials, the activity ratios measured and the insulin half-life determined. Incorporation of

[^{3}H]leucine into total protein under high glucose over 24 h was determined by precipitation with trichloroacetic acid (TCA). The data is expressed as the ratio of radiolabeled (pro)insulin/TCA precipitated protein.

Cathepsin D Activity

To measure cathepsin D activity, 1.0×10^4 cells were thoroughly washed in glucose-free Hank's solution and dissolved by sonication in 200 mL acetate-EDTA buffer (1.1 mmol/L

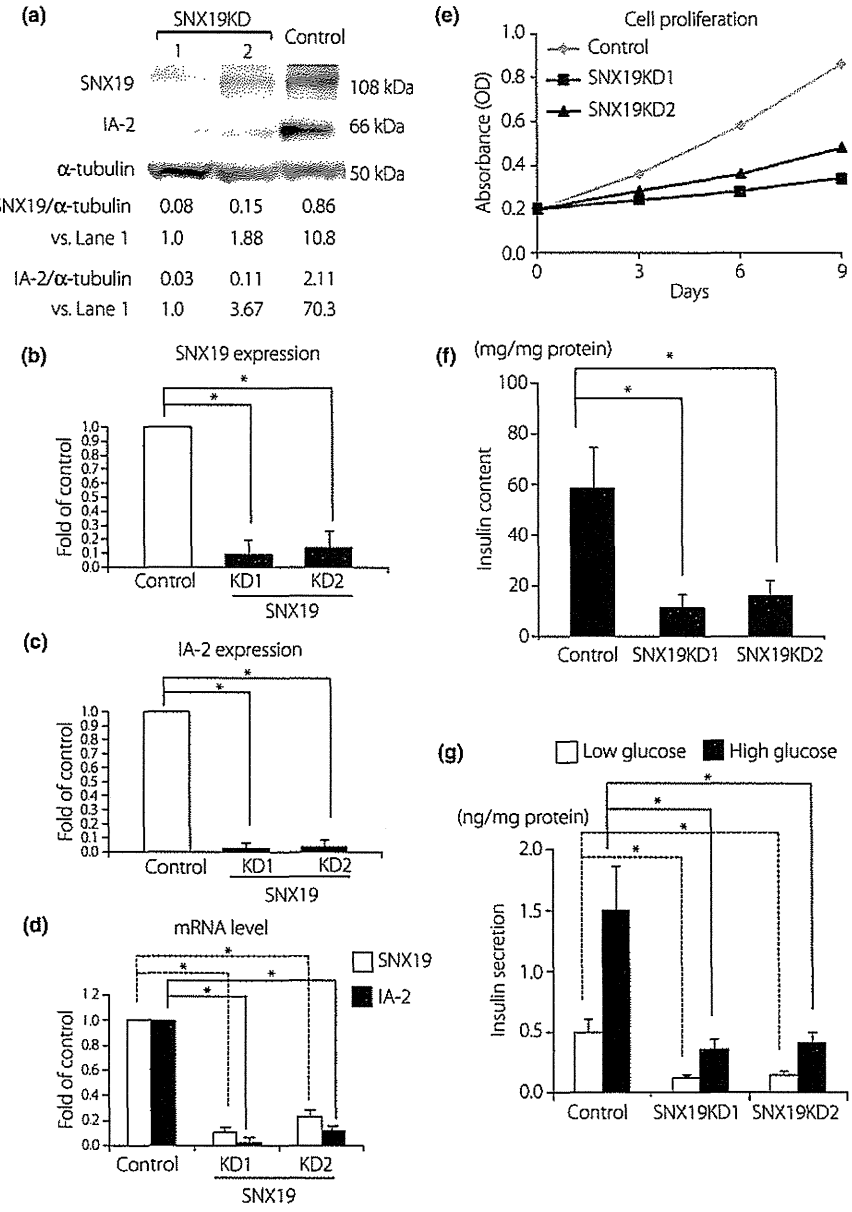

Figure 1 | Decrease in sorting nexin 19 (SNX19) expression slowed cell proliferation and reduced insulin content and insulin secretion. (a) Establishment of SNX19 knockdown MIN6 cells. Western blot analysis of SNX19 and insulinoma-associated protein 2 (IA-2) expression in sorting nexin 19 knockdown (SNX19KD) and control MIN6 cells. (b) Relative ratio of SNX19 expression in SNX19KD MIN6 cells compared with that in control MIN6 cells. (c) Relative ratio of IA-2 expression in SNX19KD MIN6 cells compared with that in control MIN6 cells. (d) Relative ratio of mRNA level of SNX19 or IA-2 quantified by real time polymerase chain reaction in SNX19KD MIN6 cells compared with that in control MIN6 cells. (e) Cell proliferation measured by a bromodexyuridine cell proliferation assay in control, SNX19KD MIN6 cells. (f) Insulin content in control and SNX19KD MIN6 cells. (g) Low (3 mmol/L) and high (25 mmol/L) glucose-stimulated insulin secretion in control and SNX19KD MIN6 cells. Images are representative of three independent experiments. Data are means ± SE of four independent experiments. *$P < 0.01$.

EDTA, 5 mmol/L acetate, pH 5.0). Aliquots were used to measure lysosomal activity determined by cathepsin D activity kit (Sigma).

Statistical Analysis

All data are expressed as mean ± standard error. Student's *t*-test was used to determine statistical significance.

RESULTS

Knockdown of SNX19 Decreases Insulin Content and Insulin Secretion in MIN6 cells

We established two permanent SNX19 knockdown (SNX19KD) MIN6 cell lines (SNX19KD1 and SN19KD2). Western blot showed that SNX19 expression was decreased to approximately one-tenth and one-fifth in SNX19KD1 and SNX19KD2 MIN6 cells, respectively, compared with that in scrambled siRNA-expressing MIN6 cells (control; Figure 1a,b). IA-2 expression was decreased to less than one-thirtieth in SNX19KD1 and SNX19KD2 MIN6 cells compared with that in control MIN6 cells (Figure 1a,c). Quantitative real-time PCR showed that messenger RNA level of SNX19 was decreased by approximately one-tenth and one-fifth in SNX19KD1 and SNX19KD2 MIN6 cells, respectively (Figure 1d). Messenger RNA level of IA-2 also was decreased by one-thirtieth and one-tenth in SNX19KD1 and SNX19KD2 MIN6 cells, respectively, as observed in western blot (Figure 1d). Cell proliferation of the SNX19KD cells were decreased by approximately one-third to one-quarter compared with that of control cells (Figure 1e). As a reduction in IA-2 expression and cell proliferation in pancreatic β-cells is known to decrease insulin content and secretion[9,14], we examined insulin content and glucose-stimulated insulin secretion in SNX19KD MIN6 cells. Insulin content was

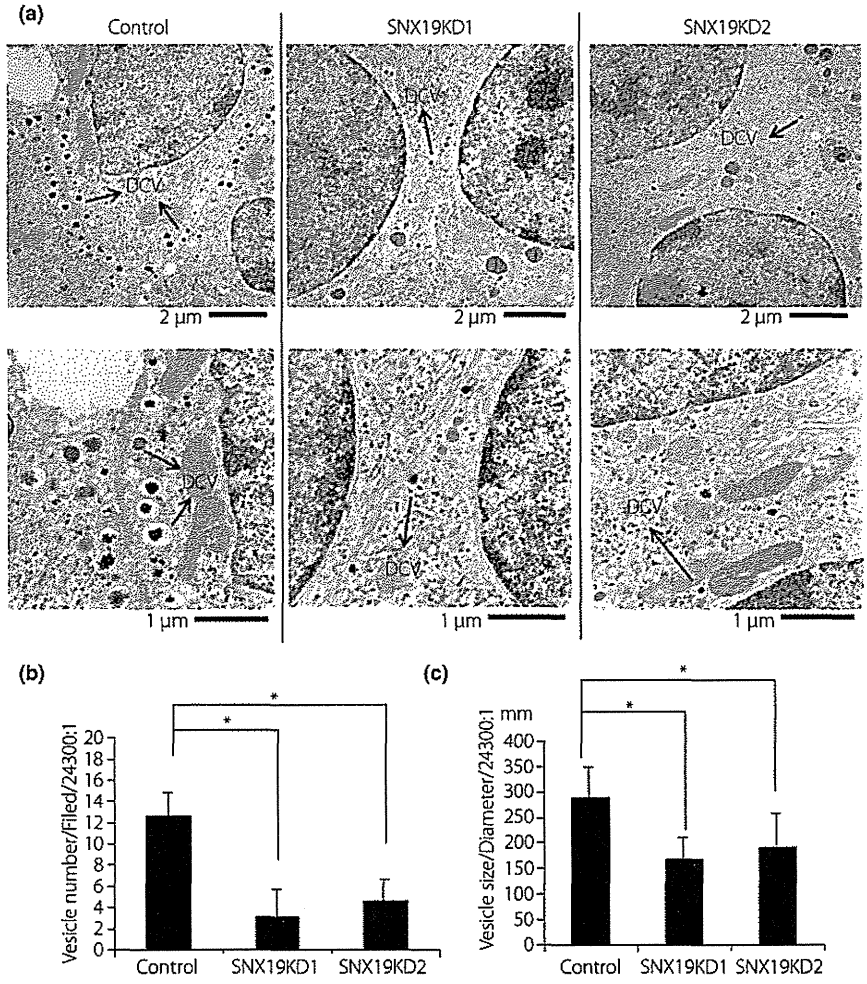

Figure 2 | Knockdown of sorting nexin 19 (SNX19) decreased the number of dense core vesicles (DCV). (a) Representative electron micrographs of 15 images in control, sorting nexin 19 knockdown (SNX19KD)1 and SNX19KD2 MIN6 cells. Black arrows indicate DCV. (b) Average number of DCV in control, SNX19KD1 and SNX19KD2 MIN6 cells. (c) Average size of DCV in control, SNX19KD1 and SXN19KD2 MIN6 cells. Data are means ± SE of four independent experiments. *$P < 0.01$.

decreased to one-seventh and one-quarter in SNX19KD1 and SNX19KD2 MIN6 cells, respectively, compared with that in control MIN6 cells (Figure 1f). The amounts of constitutive and glucose-stimulated insulin secretion also were decreased to approximately one-quarter and one-third in SNX19KD1 and SNX19KD2 cells, respectively, compared with that in control MIN6 cells (Figure 1g). These results suggest that SNX19 regulates insulin content and insulin secretion with a decrease in IA-2 expression.

Knockdown of SNX19 Decreases the Number and the Size of DCV in MIN6 Cells

We then examined the number of DCV in SNX19KD MIN6 cells. Electron micrographs showed that the number of DCV

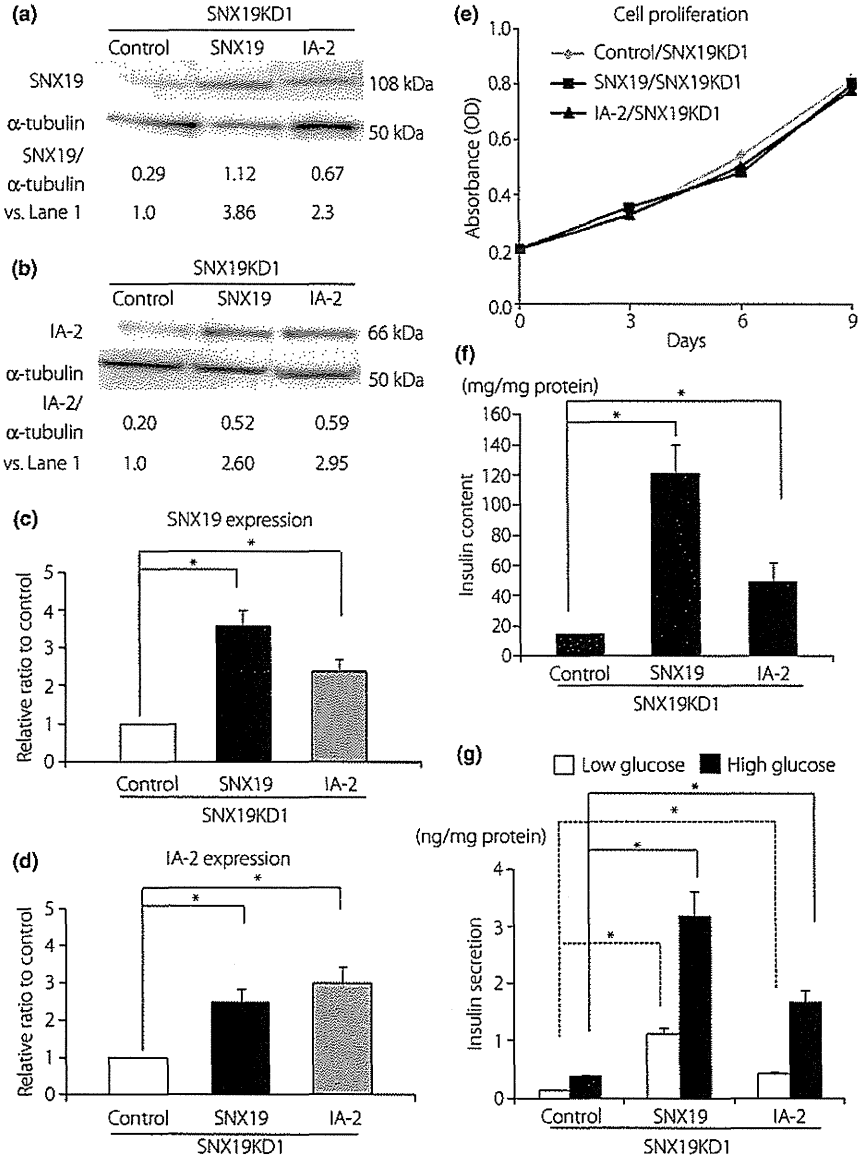

Figure 3 | Reintroduction of sorting nexin 19 (SNX19) or insulinoma-associated protein 2 (IA-2) in sorting nexin 19 knockdown (SNX19KD) MIN6 cells restored cell proliferation rate, insulin content and insulin secretion. (a) Western blot analysis of SNX19 expression in control, SNX19/ and IA-2/SNX19KD1 MIN6 cells. (b) Western blot analysis of IA-2 expression in control, SNX19/ and IA-2/SNX19KD1 MIN6 cells. (c) Relative ratio of SNX19 expression in SNX19/ and IA-2/SNX19KD1 MIN6 cells compared with that in control/SNX19KD1 MIN6 cells. (d) Relative ratio of IA-2 expression in SNX19/ and IA-2/SNX19KD1 MIN6 cells compared with that in control/SNX19KD1 MIN6 cells. (e) Cell proliferation measured by a bromodexyuridine cell proliferation assay in control/, SNX19/ and IA-2/SNX19KD1 MIN6 cells. (f) Insulin content in control/, SNX19/ and IA-2/SNX19KD1 MIN6 cells. (g) Low (3 mmol/L) and high (25 mmol/L) glucose-stimulated insulin secretion in control/, SNX19/ and IA-2/SNX19KD1 MIN6 cells. Images are representative of three independent experiments. Data are means ± SE of four independent experiments. *$P < 0.01$.

was dramatically decreased in SNX19KD1 and SNX19KD2 MIN6 cells compared with that in control cells (Figure 2a). In addition, the size of DCV was smaller in SNX19KD1 and SNX19KD2 MIN6 cells compared with that in control cells (Figure 2a). The average number of DCV was decreased to approximately one-sixth and one-quarter in SNX19KD1 and SNX19KD2 MIN6 cells, respectively, compared with that in control cells (Figure 2b). The size of DCV in SNX19KD1 and SNX19KD2 MIN6 cell lines were also decreased by approximately 40 and 35%, respectively, compared with that in control cells (Figure 2c).

Reintroduction of SNX19 and IA-2 in SNX19KD MIN6 Cells Restores Insulin Content and Insulin Secretion

To confirm the effect of SNX19 on the number of DCV, we used established permanent human SNX19-reintroduced SNX19KD1 (SNX19/SNX19KD1) MIN6 cells and human IA-2-reintroduced SNX19KD1 (IA-2/SNX19D1) MIN6 cells. Western blot analysis showed that SNX19 expression was increased by fourfold in SNX19/SNX19KD1 cells and by approximately twofold in IA-2/SNX19KD1 cells, respectively, compared with that in control vector-transfected SNX19KD1 cells (control/SNX19KD1; Figure 3a,c). In addition, IA-2 expression was

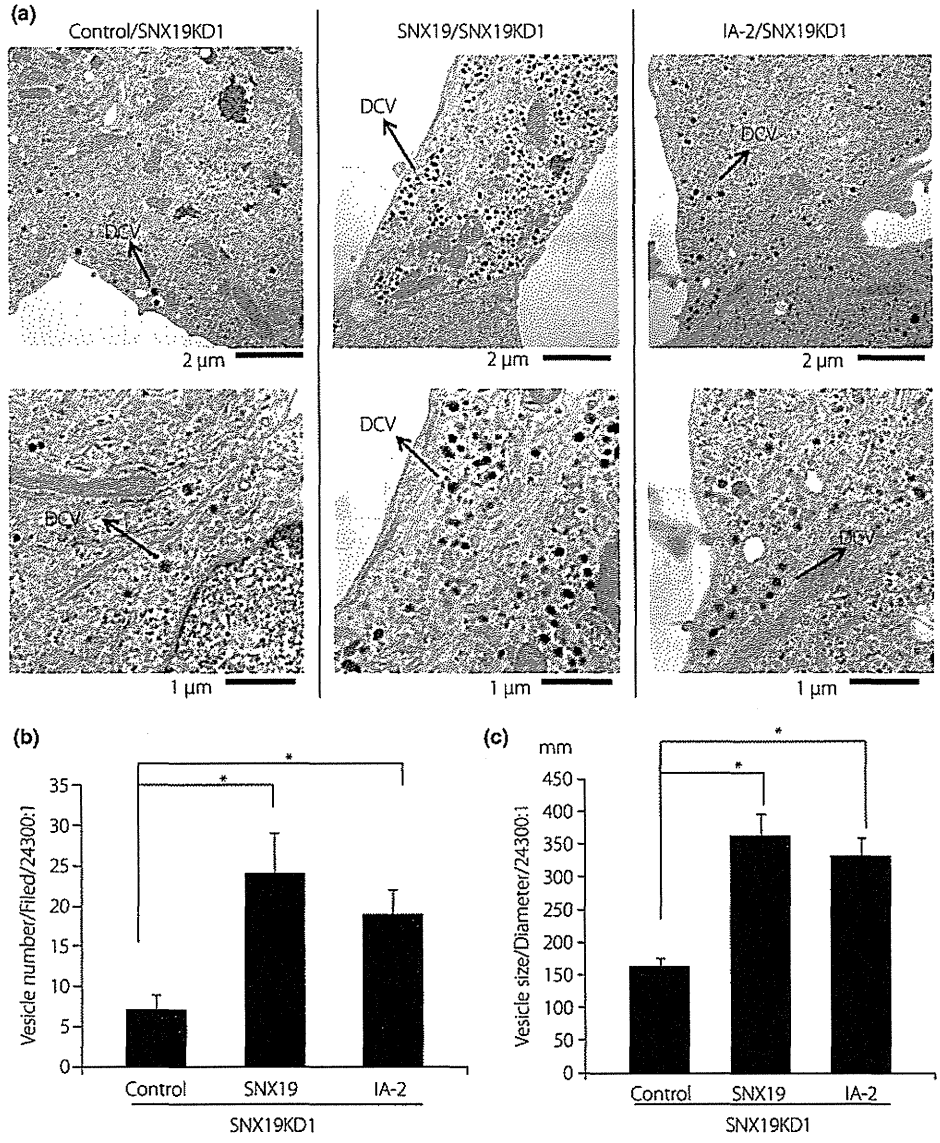

Figure 4 | Reintroduction of sorting nexin 19 (SNX19) or insulinoma-associated protein 2 (IA-2) restored the number of dense core vesicles (DCV). (a) Representative electron micrographs of 15 images in control, SNX19/ sorting nexin 19 knockdown (SNX19KD)1 and IA-2/SNX19KD1 MIN6 cells. Black arrows indicate DCV. (b) Average number of DCV in control, SNX19/SNX19KD1 and IA-2/SNX19KD1 MIN6 cells. (c) Average size of DCV in control, SNX19/SNX19KD1 and IA-2/SXN19KD1 MIN6 cells. Data are means ± SE of four independent experiments. *$P < 0.01$.

increased by approximately 2.5-fold in SNX19/SNX19KD1 MIN6 cells and approximately threefold in IA-2/SNX19KD1 MIN6 cells, respectively (Figure 3b,d). Cell proliferation of SNX19/SNX19KD1 and IA-2/SNX19KD1 MIN6 cells were almost the same as that of control/SNX19KD1 MIN6 cells (Figure 3e). Accordingly, insulin content was increased by approximately sevenfold and threefold in SNX19/SNX19KD1 and IA-2/SNX19KD1 cells, respectively, compared with that in control/SNX19KD1 cells (Figure 3f). Constitutive and glucose-stimulated insulin secretion also were increased by approximately sixfold and threefold in SNX19/SNX19KD1 and IA-2/SNX19KD1 cells, respectively, compared with those in control/SNX19KD1 cells (Figure 3g).

Reintroduction of SNX19 and IA-2 Increases the Number and the Size of DCV in SNX19KD MIN6 Cells

Electron micrographs showed that the number of DCV was increased in both SNX19/SNX19KD1 and IA-2/SNX19KD1 MIN6 cells compared with that in control/SNX19KD1 cells (Figure 4a). The number of DCV was increased by approximately fourfold in SNX19/SNX19KD1 cells and approximately threefold in IA-2/SNX19KD1 cells, respectively, compared with that in control/SNX19KD1 cells (Figure 4b). The size of DCV was increased by approximately twofold in both SNX19/SNX19KD1 and IA-2/SNX19KD1 cells compared with that in control/SNX19KD1 MIN6 cells (Figure 4c).

SNX19 Affects the Half-life of DCV

To investigate the involvement of SNX19 in DCV stability, we measured the half-life of DCV in SNX19KD1 and SNX19/SNX19KD1 cells. A pulse-chase experiment showed that the half-life of DCV in SNX19KD1 cells was 11.6 h, approximately half of that in control cells (Figure 5a). In contrast, the half-life of DCV in SNX19/SNX19KD1 was 30.4 h, approximately threefold of that in control/SNX19KD1 cells (Figure 5b). To ascertain that the decreased half-life of DCV in SNX19KD1 cells was not the result of a decrease in biosynthesis of proinsulin/insulin, cells were pulsed with [^{3}H]leucine, and newly synthesized proinsulin/insulin was measured. At the end of a 24-h pulse, the amount of proinsulin/insulin in SNX19KD1 cells was almost equal to or slightly lower than that in control cells (Figure 5a). Similarly, the amount of newly synthesized proinsulin/insulin in SNX19/SNX19KD1 cells was almost equal to or slightly greater than that in control/SNX19KD1 cells (Figure 5b). These results show that SNX19 stabilizes DCV.

SNX19 Knockdown Increases the Activity of Lysosomes

The finding that SNX19 affected the half-life of DCV suggested that the reduction of DCV number in the SNX19KD cells might be the result of accelerated DCV degradation. The number of lysosomes in SNX19KD1 cells was increased by approximately fourfold compared with that in control MIN6 cells (Figure 6a,b). In contrast, the number of lysosomes in SNX19/SNX19KD1

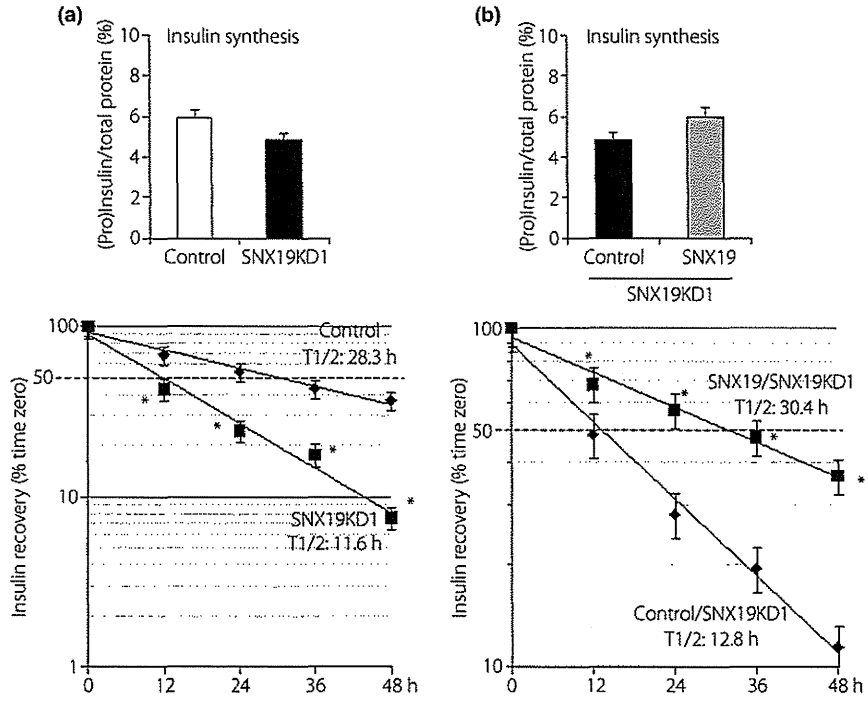

Figure 5 | Sorting nexin 19 (SNX19) affected the half-life of dense core vesicles (DCV). (a) Half-life of DCV and insulin and proinsulin biosynthesis in control and sorting nexin 19 knockdown (SNX19KD)1 MIN6 cells; (b) in control/ and SNX19/SNX19KD1 MIN6 cells. Data are means ± SE of four independent experiments. *$P < 0.01$.

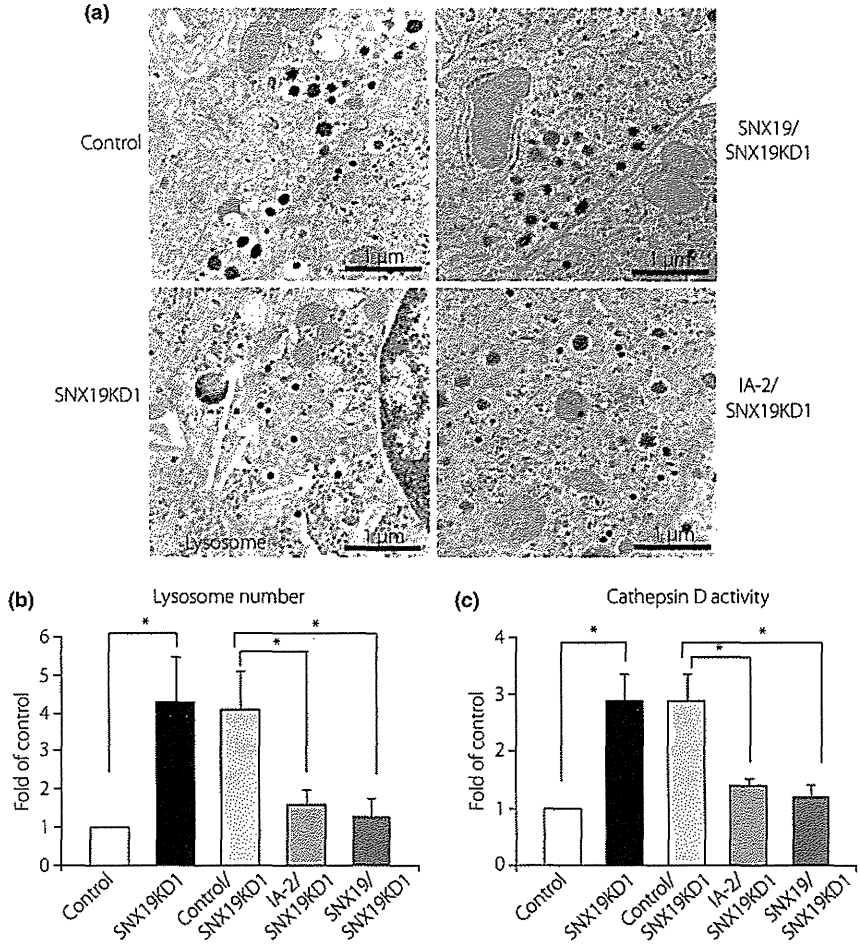

Figure 6 | Decreased expression of sorting nexin 19 (SNX19) increased activity of lysosomes and autophagy. (a) Representative electron micrographs of 15 images in control, sorting nexin 19 knockdown (SNX19KD)1, IA-2/SNX19KD1 and SNX19/SNX19KD1 MIN6 cells. White arrows indicate lysosomes. (b) Average lysosome number per image of 20 images. (c) Cathepsin D activity. Data are means ± SE of four independent experiments. *$P < 0.01$.

and IA-2/SNX19KD1 cells was almost equal to that in control cells and less than one-third of that in control/SNX19KD1 cells (Figure 6a,b). Activity of lysosome enzyme cathepsin D also was increased by approximately threefold in SNX19KD1 cells compared with that in control cells (Figure 6c), whereas activity of cathepsin D in IA-2/ and SNX19/SNX19KD1 cells was decreased to approximately half of that in control/SNX19KD1 cells (Figure 6c).

DISCUSSION

The experiments reported in the present study show that knockdown of SNX19 decreases the number of DCV in MIN6 cells, and also decreases the cellular content and secretion of insulin. Conversely, reintroduction of SNX19 increases the number of DCV in MIN6 cells, and increases the cellular content and secretion of insulin. Thus, SNX19 expression is regulated at the transcriptional level and affects the half-life of DCV, insulin content and secretion. The half-life of DCV in SNX19KD cells was 11.6 h as compared with 28.3 h in control cells and reintroduction of SNX19 increased the half-life of DCV in SNX19KD cells from 12.8 to 30.4 h. The most likely explanation for these findings is that the reduced half-life of the DCV is responsible for their reduced number, which directly underlies the decrease in insulin content and secretion.

Of particular interest, earlier experiments showed that overexpression of IA-2 in MIN6 cells significantly increased the half-life of the DCV, as well as the content and secretion of insulin[14]. Indeed, a very recent experiment found that IA-2 or IA-2β single knockout and IA-2/IA-2β double knockout mice showed a significant decrease in the number of DCV and the content and secretion of insulin (Cai T and Notkins AL, unpublished data, 2011).

IA-2 and IA-2β are transmembrane proteins on the DCV and it is thought that knockout (Cai T and Notkins AL,